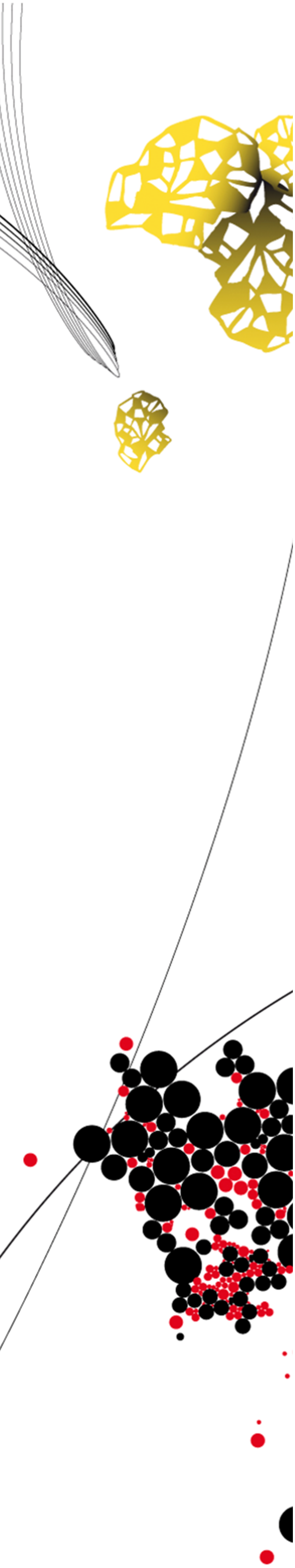

UNIVERSITY OF TWENTE.

Faculty of Science and Technology

Investigation of immiscible liquid-liquid displacement in Slippery Liquid Infused Membranes (SLIM)

Jaap Eijsker
BSc Thesis
26-06-2017

Supervisor:
Prof. dr. ir. R.G.H. Lammertink
Daily supervisor:
Hanieh Bazyar

Soft Matter, Fluidics and Interfaces Group (SFI)
Faculty of Science and Technology,
University of Twente
P.O. Box 217
7500 AE Enschede
The Netherlands

---

1 Abstract

A bachelor assignment was performed with the Soft matter, Fluidics and Interfaces (SFI) group at the University of Twente. Research is being carried out on slippery liquid infused membranes (SLIMs): the presence of an intermediary, immiscible liquid prevents direct contact between the permeate and the membrane wall by coordinating multiphase transport through the pores. It has been shown that these systems exhibit promising anti-fouling properties for relatively clean water.

The goal of the assignment: to learn more about the stability of SLIMs under more extreme conditions, i.e. surfactant solutions. In this research, porous PVDF membranes are fabricated, characterised using SEM and gas-liquid displacement porometry and infused with slippery liquids (Krytox 101 or silicone oil AR20). Most importantly, liquid-liquid displacement (LLDP) experiments are performed with several non-ionic and ionic surfactant solutions to observe the stability of the system. These surfactants are Triton X100 (non-ionic), SDS (anionic), CTAB (cationic) and DDAPS (zwitterionic), common surfactants below or at CMC. Finally, the LLDP measurements are reproduced using a microfluidic chip and a Laser Confocal Scanning Microscope (LCSM), to observe and analyse the displacement phenomenon that occurs with surfactant solutions in SLIMs.

The SLIM stability with surfactant solutions is demonstrated. The LCSM experiments reveal a swift removal of the oil bulk, but a final saturation value of water below 100% that is rather stable (between 0.8 and 0.95, depending on the displacing surfactant solution). Likewise, the LLDP results confirm that a certain amount of infusion liquid is retained up to the highest fluxes for all surfactant solutions.

Contents

2 Introduction

Direct contact of regular membranes with liquid permeate can often result in membrane fouling. Depending on the operation time, prevention of membrane fouling can result in energy savings of over 50%. [1] A possible bio-inspired solution for fouling is the creation of a synthetic liquid-repellent surface (superhydrophobic surface). [2] Synthetic superhydrophobic surfaces show promising self-cleaning properties. [3]
The liquid-repellent properties of these microtextured surfaces depend on the formation of stable air pockets. However, after years of investigation, these surfaces still present problems that have been proven difficult to resolve: the stable air-liquid interface required for liquid-repulsion is easily disrupted by physical damage to the surface, impacting liquid droplets and increased pressures. Furthermore, a high contact angle hysteresis is observed. These problems can be tackled by creating slippery liquid-infused surfaces that do not rely on air pockets, making them stable at pressures of up to 680 atm. Additionally, these surfaces show fast self-healing abilities (0.1 - 1 s after physical damage), omniphobicity (repulsion of water, hydrocarbons and crude oil) and low contact angle hysteresis ($< 2.5°$). [2]

2.0.1 Wetting and hydrophobicity

Wetting can be considered as liquid coverage over a solid. The degree of wetting can be described by the equilibrium contact angle θ_C, as shown for water in Figure 1a. Wetting decreases as the contact angle increases: a surface is said to be superhydrophobic when water droplets exhibit a contact angle of $\theta_C > 150°$ (Figure 1b). [4]

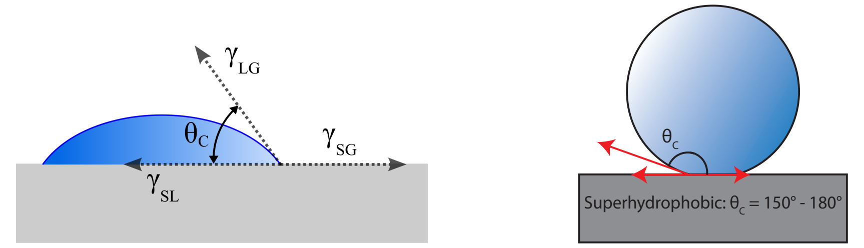

(a) Schematically: a water droplet on a solid surface. [5]

(b) Typical contact angles for superhydrophobic surfaces. [6]

Figure 1: Contact angles for droplets on a solid substrate.

The inspiration for creating a synthetic superhydrophobic surface comes from nature: lotus leaves show excellent water repulsion ($\theta_C > 150°$) and self-cleaning properties (the "lotus effect"), the combined result of a natural hydrophobic wax and micro/nanoscale surface roughness, see Figure 2. [3]
However, the mentioned stability problems of these surfaces have lead to the investigation of another bio-inspired solution: liquid infused slippery surfaces, as found in pitcher plants. Like with lotus leaves, the surface roughness that pitcher plants exhibit is the key to liquid repulsion. However, the surface of pitcher plants uses its roughness to incorporate an intermediary liquid (Figure 3b), which is then capable of repelling water, as opposed to the direct repulsion by lotus leaves. [3] Both leaves are shown in Figure 2, as well as a synthetic superhydrophobic surface.

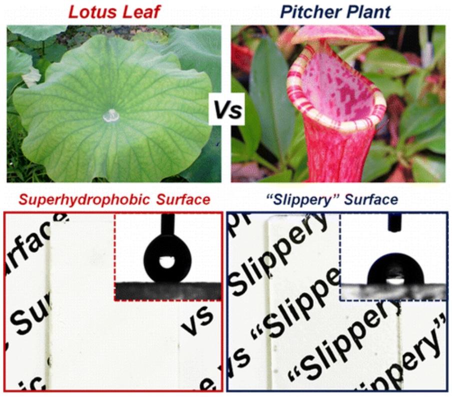

Figure 2: A lotus leaf and pitcher plant, with below their artificial counterparts: a surface with nanoscale roughness (left), which was infused with silicone oil (right). Water droplets exhibit a contact angle of 150° (left) and 96° (right). [3]

2.0.2 Slippery surfaces

The intermediary liquid in slippery liquid infused surfaces addresses several issues of the non-infused superhydrophobic surfaces. First of all, the liquid infusion shows a significantly better pressure stability than the air-liquid interface of superhydrophobic surfaces. For instance, some slippery liquid infused membranes (SLIM) maintain their liquid repelling abilities up to pressures of at least $\approx 676\ atm$, while the pressure stability record for superhydrophobic surfaces with water is $\approx 7\ atm$.
The air-liquid interface can be depicted using the Cassie-Baxter model for superhydrophobic surfaces, as shown in Figure 3a. [7] In the case of liquid infusion, the air pockets are infiltrated with the infusion liquid (see Figure 3b), resulting in the observed stability and a smaller equilibrium contact angle, in the range of $93^\circ < \theta_C < 136^\circ$ for PVDF membrane surfaces (polyvinylidene fluoride) [8].

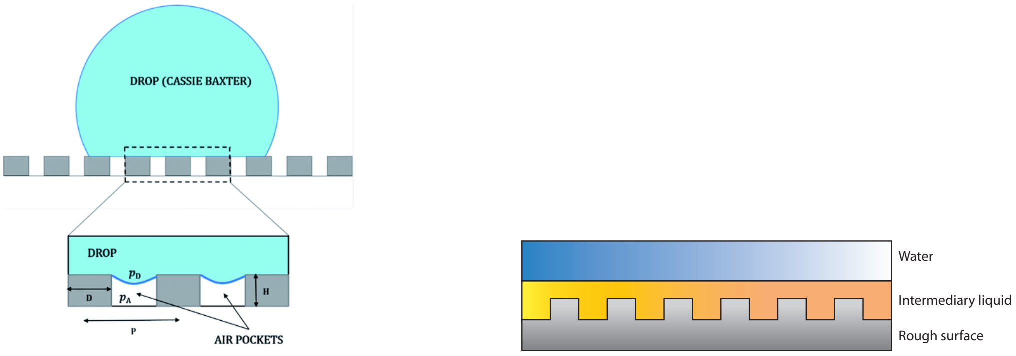

(a) Cassie-Baxter state of a liquid drop on a rough surface. [7]

(b) A slippery liquid infused rough surface.

Figure 3: Schematically: Cassie-Baxter state (a) and liquid infusion of the air pockets (b).

Furthermore, the liquid layer provides a smooth, chemically homogeneous surface without defects. This allows for a very small contact angle hysteresis ("the difference between the advancing and receding contact angles of a moving droplet" [2]). The contact angle hysteresis (CAH, Figure 4) is a measure of slipperyness: the low CAH means that water droplets have high mobility on the surface (little to no "pinning" occurs) and good, slippery behaviour is achieved. [2]

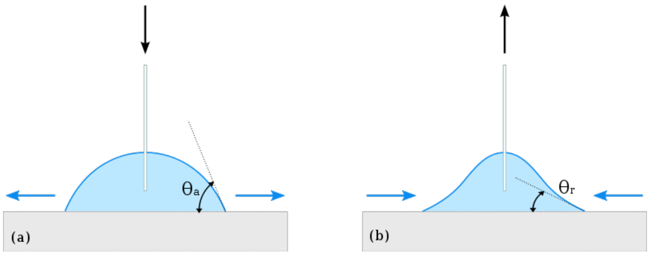

Figure 4: Contact Angle Hysteresis (CAH) shown schematically as the difference between the "advancing" angle (θ_a, a) and the "receding" angle (θ_r, b). [9] CAH is often measured by increasing (for θ_a) and decreasing (for θ_r) the droplet volume using a needle.

The creation of SLIMs is achieved by infiltrating a porous membrane with infusion liquid. Another advantage of the liquid infusion approach is its independency of the substrate's geometry, which makes it applicable to a wide range of hydrophobic materials, like Teflon [2] or PVDF membranes [8]. In the case of PVDF membranes, the contact angle hysteresis decreases from $\text{CAH} = 25^\circ$ to a range of $4.1^\circ < \text{CAH} < 6.2^\circ$ in the case of liquid infusion, depending on the liquid. [8] The infusion of the slippery liquid is based on well-matched solid and liquid surface energies, combined with microtextural roughness. The infused liquid is stabilized by capillary forces. Additionally, the infusion liquid (the lubricant) should be immiscible with the influent liquids. [2]
The protective liquid lining in a SLIM can coördinate multiphase transport and prevent fouling by means of a gating mechanism, shown in Figure 5.

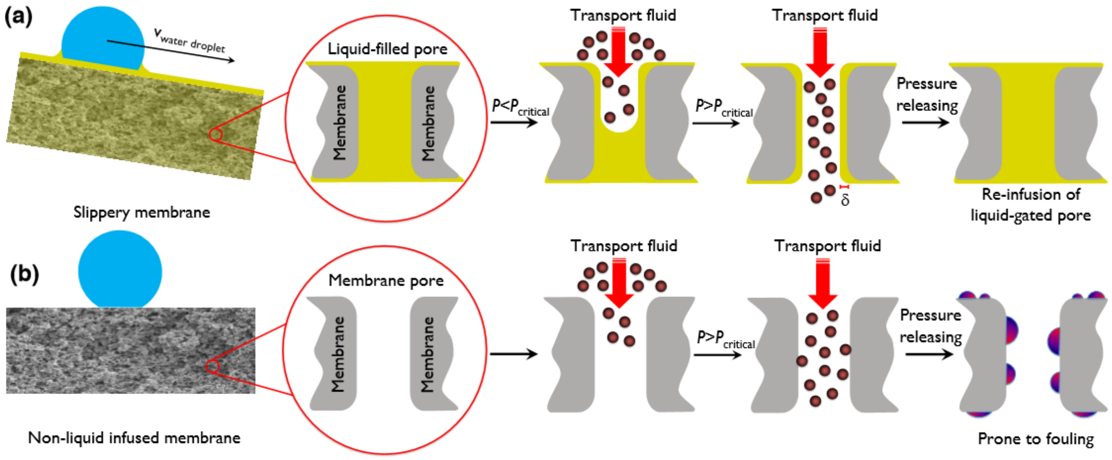

Figure 5: Schematic depiction of the gating mechanism occurring in slippery membranes (a) which can prevent fouling, as opposed to non-liquid infused membranes (b). [10]

2.0.3 Objective

In this research, the surfaces to be investigated are PVDF membranes infused with respectively a silicone oil and a fluorinated oil; SLIMs. [10] Liquid-liquid displacement porometry (LLDP) experiments, where pure water is pushed (flux controlled) through a PVDF membrane infused with perfluoropolyether oil (Krytox 101), have demonstrated the stability of this system. However, the infused membrane has not yet been tested in more extreme conditions.

LLDP (constant flux) will be performed for dry, prewet and slippery liquid infused membranes, with surfactant solutions at concentrations below or near the critical micelle concentration (CMC). [10] The CMC is the surfactant concentration above which the surface tension of a liquid becomes independent of the surfactant's concentration, due to the formation of micelles. [4]
The slippery liquids used for this are Krytox 101 and silicone oil AR20. The used surfactants are Triton X100 (non-ionic), SDS (anionic), CTAB (cationic) and DDAPS (zwitterionic). More explanation about surfactants and CMC can be found in Section 2.1.3. By comparing the porometry results with those of dry and prewet membranes, the SLIM performance can be studied for different surfactants. Also, the experimental data is fitted to the Interfacial Pore Flow model.

In addition to the liquid-liquid displacement porometry, the displacement behaviour will be observed using a microfluidic chip and laser confocal scanning microscopy (LCSM).
Furthermore, new PVDF membranes will be synthesised in order to get more acquinted with membrane technology. These membranes will then be characterized using SEM (see Section 3.3.1) and gas flow porometry (see Section 3.3.2).

2.1 Background theory

2.1.1 Surface Tension and Interfacial Tension

One can distinguish between two kinds of interfaces: fluid interfaces and non-fluid or solid interfaces. Fluid interfaces can be gas-liquid or liquid-liquid interfaces. [4] Usually, gas-liquid interfaces are referred to as *surfaces.*

Surface tension
As an example, the case of a water-air surface is considered. In this case, surface tension (SFT) is the result of imbalanced forces between water molecules attracting each other and water molecules interacting with air, as depicted in Figure 6. The consequence of this imbalance is a net force inward, directed at the bulk of the fluid. [4] This force can be observed as *tension* and gives rise to a water droplet's tendency to minimise its surface area.

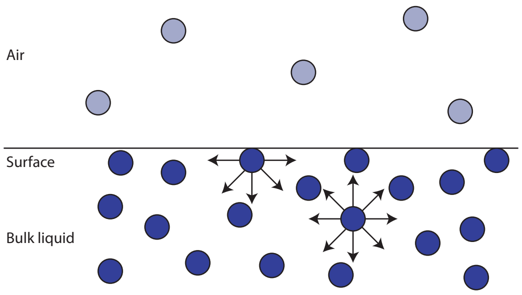

Figure 6: Surface tension of water in air visualised. [4]

Interfacial tension
Interfacial tension is much like surface tension, but the term is used to describe (i.a.) liquid-liquid interfaces. As is the case with surface tension, interfacial tension is also caused by imbalanced interactions, for example in an oil-water system where water molecules interact differently with each other than with oil molecules.

Unit
Surface tension and interfacial tension are the forces per unit of length in respectively a surface and an interface. This can be summarised mathematically as $\gamma = \frac{F}{\delta x}$. The γ is commonly denoted in mN m^{-1}. [4]

2.1.2 Convective fluid transport

Laplace pressure
Curved surfaces and interfaces are caused by a pressure difference between phases. For example, the pressure in phase α in Figure 7 is bigger than that of phase β, which causes this curvature. The pressure difference at equilibrium can be related to the curvature with the Laplace equation, see Equation 1. Here, ΔP is the pressure difference in Pa, γ is the surface tension in N/m and r is the interface radius in m. In the case of symmetrical membrane pores, the interface radius is equal to the pore radius ($\mathrm{r_p}$). The Laplace equation can also be used to determine the *critical pressure* required for opening a pore. In the example of Figure 7, $P^\alpha > P^\beta$ is required for phase α to proceed through the depicted cylinder. From the Laplace equation, it becomes clear that a larger γ results in higher equilibrium pressures. This means a higher pressure is required to open the same pores if γ increases. [4]

$$P^\alpha - P^\beta = \Delta P = \frac{2\gamma}{r} \tag{1}$$

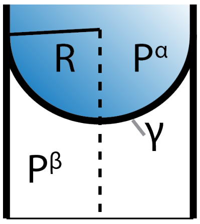

Figure 7: Schematically: a curved interface.

However, the above only holds when perfect wetting with the cylinder wall is achieved. If this is not the case, for example when a water droplet moves through the pores of a hydrophobic membrane, the contact angle θ with the wall needs to be taken into account. The Laplace equation then becomes: [4]

$$\Delta P = \frac{2\gamma \cos\theta}{r_p} \tag{2}$$

It can be seen that the equation still holds for perfect wetting. In that case, contact angle θ becomes 0°, effectively eliminating the cosine factor.

Hagen-Poiseuille flow
After membrane pores have been opened, the convective fluid transport through them continues, but another model is needed to describe this. The Hagen-Poiseuille model for fluid transport through cylindrical pores is regularly used do describe this, see Equation 3 [11].

$$J_i = \frac{N_i \pi r_i^4}{8\eta l} \Delta P \tag{3}$$

Here, N_i $(pore/m^2)$ is the density of pores with radius r_i (m), η (Pa s) is the dynamic viscosity of the transport fluid. Δ P is the applied pressure on the membrane (Pa) and l is the length of the pores, which should take tortuosity into account.

Permeability
The permeability of a membrane to a certain fluid can be calculated using Darcy's law, see Equation 4. [8]

$$Q = \frac{kA}{\mu} \frac{\delta p}{\delta x} \tag{4}$$

Here, Q (m^3/s) is the volumetric flow of the displacing fluid k (m^2) is the permeability, A (m^2) is the cross-sectional area of the sample, μ $(Pa\ s)$ is the dynamic viscosity of the displacing fluid. $\frac{\delta p}{\delta x}$ is the pressure gradient in the membrane (Pa/m) [8], so the pressure difference across the membrane divided by its thickness.

2.1.3 Surfactants

Surfactants (an abbreviation for surface active agents) are water-soluble amphiphiles. Amphiphiles are molecules that contain both a hydrophilic and a hydrophobic (or oleophilic) component. If an amphiphile is strongly adsorbed at surfaces, it is called a surfactant. [4] Surfactants present at surfaces because of their dual nature: in the example of a water surface, the hydrophilic part of a surfactant will be located in the water, while the hydrophobic part prefers to be in the vapour phase (air). In general, the hydrophilic part of a surfactant is called the head and the hydrophobic part the tail.

Surfactants can be divided into four categories: non-ionic, anionic, cationic and zwitterionic. Anionic surfactants possess a negatively charged (hydrophilic) head, whereas cationic surfactants possess a positively charged (hydrophilic) head. An example of an anionic surfactant is shown in Figure 8. Note the large hydrocarbon chain that forms the hydrophobic (or oleophilic) tail, and the polar hydrophilic head. Zwitterionic surfactants possess both a negative and a positive charge in the molecule.

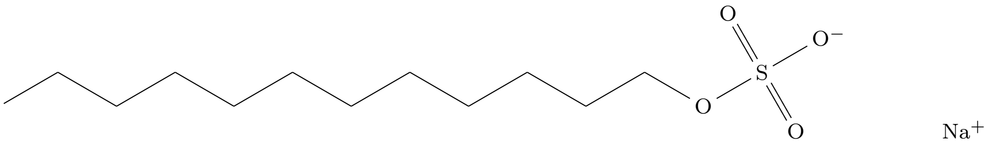

Figure 8: Dissolved sodium dodecyl sulphate (SDS), a common anionic surfactant.

The surface tension of a surfactant solution depends on its concentration. A higher concentration of surfactants results in a lower γ. However, there is a limit to this dependence: after a certain critical concentration, micelles start to form and additional amounts of surfactant are not adsorbed at the surface anymore. Micelles are spherical aggregates of surfactant molecules; energy is minimised by forming a surface layer of the hydrophilic heads (in water), while the hydrophobic tails avoid contact with the water by sticking together. [4] This is depicted in Figure 9.

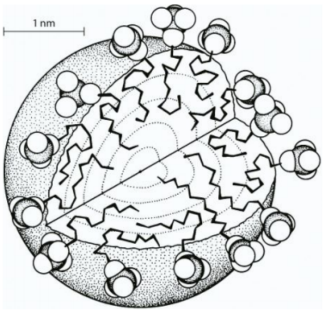

Figure 9: Schematically: SDS molecules forming a micelle in water. [4]

Marangoni stress
A surface with a gradient in surfactant concentration also exhibits differences in surface tension. This can be

caused by temperature or composition differences. If the arising gradient in surface tension is sufficiently large to overcome viscous and inertial forces, liquid displacement is observed: Marangoni convection. [4]

Emulsions

Emulsions arise when droplets of one liquid phase are dispersed in another, for example oil droplets in water. Emulsions are often formed with the help of surfactants (*emulsifiers*). These emulsifiers increase the stability of droplets in several ways. Statically, the interfacial tension is reduced, which decreases the thermodynamic tendency to minimise the surface area by forming just one interface (instead of many droplet interfaces). Also, the surfactant molecules physically hinder breaking an emulsion.

The surfactants also have a dynamic effect on the emulsion. If e.g. two oil droplets approach each other, the convective water outflow causes a local dilution of surfactant molecules. Because of this, the Marangoni effect results in the surfactants' tendency to flow back and drag water along, which discourages coalescence. [4] This effect is depicted in Figure 10.

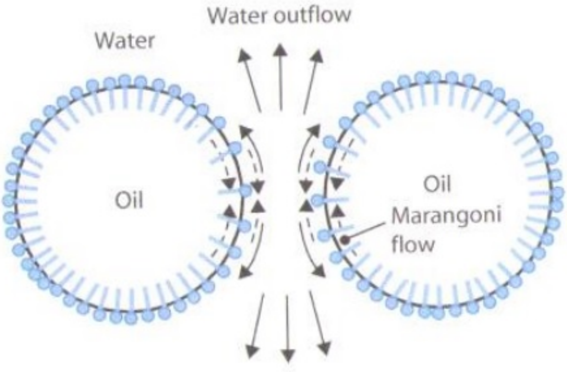

Figure 10: The effect of surfactants on emulsion stability. [4]

3 Materials and Method

3.1 Materials

PVDF (Solef 6020/1001) was received from Solvay Solexis, France. 1-methyl-2-pyrrolidinone (NMP) (99% extra pure) was purchased from Acros Organics, The Netherlands. Ethanol (99.8%) was supplied from Atlas and Assink chemical company, The Netherlands. Krytox GPL oil 101 was purchased from MAVOM chemical industry, The Netherlands. Fluorinert FC-43 was supplied from BASF chemical company, Germany. Silicone oil AR20 was purchased from Sigma-Aldrich, The Netherlands. Triton X100, Sodium Dodecyl Sulfate (SDS), N-Dodecyl-N,N-dimethyl-3-ammonio-1-propanesulfonate (DDAPS) and Hexadecyltrimethylammonium bromide (CTAB) were purchased from Sigma-Aldrich, The Netherlands.

The surfactants used are listed in Table 1 with their respective properties. The chosen surfactants are common and have different charges to show the effect of non-ionic surfactants versus ionic ones. All used surfactant concentrations are either below CMC (SDS, DDAPS) or at CMC (Triton, CTAB).

Table 1: The surfactants and their concentrations used for the measurements.

Surfactant	Charge	Concentration [mg/L]	Concentration [mmol/L]	CMC [mmol/L]
Triton X100	Non-ionic	144	0.238	0.22 - 0.24 [12]
SDS	Anionic	231	0.801	8.85 - 9.68 [13]
CTAB	Cationic	346	0.949	0.92 - 1.0 [14]
DDAPS	Zwitterionic	1006	0.300	2.0 - 4.0 [15]

Both of the oils used for the measurements are shown in Table 2.

Table 2: The oils used for the measurements and their respective properties at room temperature.

Oil	Dynamic viscosity [mPa s]	Density [g/mL]
Krytox 101 [16]	17.4	1.85
Silicone oil AR20 [17]	20	1.01

3.2 Membrane fabrication

3.2.1 Fabrication of a porous PVDF membrane

The membranes used in this research are made of poly(vinylidene fluoride), or PVDF. The solvent (and afterwards also the coagulation agent) for this process is N-methyl-2-pyrrolidone, or NMP. In order to get more acquainted with membrane technology, multiple PVDF membranes were synthesized and characterized using SEM (Scanning Electron Microscope) and (capillary flow) porometry.
The polymer (dope) solution needed for fabricating the membrane was made by dissolving powdered PVDF in NMP. The desired amount of PVDF is 15 wt%; a new solution was made by mixing 75 g of PVDF in 425 g NMP with a mechanical stirrer (500 RPM) at ≈ 80 °C overnight. After dissolving the PVDF, the resulting polymer solution is made into a thin sheet, using a 0.5 mm membrane blade to evenly spread the solution over a clean glass plate. It is noteworthy that, due to shrinkage after drying, the thickness of the membrane sheet decreases significantly: from 0.5 mm to ≈ 0.1 mm as observed with SEM.

The sheet is then directly put into a coagulation bath of 70 : 30 vol% NMP:water (Mili-Q™) for 30 minutes. Because the membrane is "shielded" on one side from the coagulation bath by the glass plate, the bottom of the membrane sheet is usually slightly less porous than the top. Furthermore, because of the contact with the glass, the bottom side of the membrane is characterized by a more flat appearance, which becomes visible with SEM imaging.
After the coagulation bath, the membrane sheet (without glass) is moved to a bath of pure ethanol, where it remains for 30 minutes. Then the membrane sheet is lifted from the glass plate and left to dry on a sheet of paper. Ideally, the membrane should be as plane as possible. However, the membrane does not dry completely evenly - partly due to circulation in the fume hood - which causes unwanted wrinkling. Uniform drying can be improved by using a porous drying paper on which to place the membrane sheet, see Figure 11.

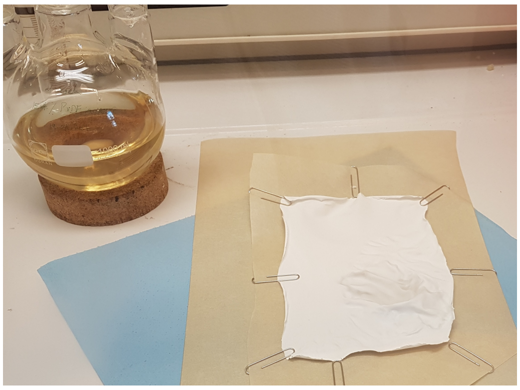

Figure 11: The polymer solution (in the round-bottomed flask) and the membrane sheet drying on paper.

Finally, the membrane is left to dry in a vacuum oven at 30 °C overnight. After that, a small circle is cut from the membrane sheet using scissors. The size is determined by the the diameter of the sample holder.

3.2.2 Creating SLIMs

The Slippery Liquid Infused Membranes are created by adding $\approx 50\ \mu$L of infusion liquid to the membrane using a micropipette, evenly distributed across the membrane surface. In this research, the infusion liquids are silicone oil (AR-20) and Krytox 101. Both oily liquids infiltrate the membrane quickly (within seconds) and spontaneously. Before any measurements of the SLIMs, the excess of infiltration liquid is removed by placing the membrane vertically for several seconds.

3.2.3 Creating prewet membrane

For each surfactant solution, liquid-liquid displacement porometry measurements were also performed on prewet membranes. These were fabricated by first infusing a dry membrane with pure ethanol (which spontaneously wicks into it), then leaving it overnight in the appropriate solution.

3.3 Membrane characterization

3.3.1 SEM

The surface of the fabricated membranes exhibits nanoroughness and other structures which are very small in size. In order to obtain a useful image of the fabricated membranes, a high spatial resolution is needed. Light-optical microscopes can achieve a maximum resolution of 0.3 μm, which makes it unsuitable for observing the surface characteristics that are mostly smaller. [18]
Because of this, Scanning Electron Microscopy (SEM) is employed, which can reach spatial resolutions of up to 1 nm for modern devices. SEM uses a very small probe to emit *primary* electrons. These primary electrons can excite atomic (*secondary*) electrons, which are then released and collected by the scanning device to form an image. Because SEM makes use of reflected electrons instead of electrons passing through a sample (which is the principle behind TEM), the sample thickness is not a problem. This, together with a large depth of focus, makes SEM the advantageous technique. [18]

In this case, a coating of 10 nm platinum was applied using a JEOL JFC-1300 sputter coating machine. The pressure was below 2 Pa (around 1 Pa). A vacuum is needed to prevent gaseous contamination and improve the sputtering process. The coating serves to prevent charging the membrane surface. A JEOL 5600 LV SEM was used at an acceleration voltage of 5 kV for the imaging.

(a) The Pt-coated bottom and top membrane samples.

(b) The Pt-coated cross-sectional membrane sample.

(c) The JEOL 5600 LV SEM that was used.

Figure 12: SEM samples and the used microscope.

3.3.2 Gas-liquid displacement porometry

For further characterization of the membrane, i.e. determining the pore size (distribution), the membrane was measured using gas flow porometry, or gas-liquid displacement porometry (GLDP). This technique is also referred to as capillary flow porometry, but that term can be used to describe both GLDP and liquid-liquid displacement porometry (LLDP). [11]

Porometry in general relies on the principle that smaller pores are more difficult to open than bigger pores, when these pores are filled with e.g. oil. For GLDP, the membrane is first infused with an infiltration liquid that should completely wet the membrane. After that, a permeating gas at increasing pressure causes an increasing number of pores to open.

In this case, the fluorinated oil FC-43 is the infiltration liquid. The permeating gas is N_2-gas. The equipment used for the GLDP measurements is the Porolux™ 1000.

The Porolux employs the Pressure Step/Stability method for its measurements. This means that the pressure is increased in very small steps. After each pressure step, the Porolux checks whether stability requirements are met for a sufficiently reliable measurement point. In other words: the algorithm waits until both the pressure and flow are stable enough to ensure that all pores of the same diameter are completely opened. [19] After all, it is possible that some pores take longer to open due to increased tortuosity. Using these pressure and flow values, the Laplace equation can be employed to calculate pore sizes, see Equation 5. [4]

$$\Delta P = \frac{2\gamma \cos\theta}{r_p} = \frac{2\gamma}{r_p} \tag{5}$$

Here, ΔP is the pressure difference in Pa, γ is the surface tension in N/m and $\mathrm{r_p}$ is the pore radius in m. The contact angle θ is equal to 0° in the case of perfect wetting, which is achieved in the case of infiltration with FC-43. After all, the fluorinated PVDF membrane is easily wetted by the fluorinated FC-43 due to well-matched surface energies. This means the contact angle factor disappears ($\cos\theta = 1$), as seen in Equation 5. Also, in this equation the pores are assumed perfectly symmetrical. Otherwise, the different curvatures of the pores would have to be taken into account. In practice, the assumption of symmetrical pores is mostly justified. The membrane structure can safely be simplified by assuming straight cylindrical pores, because the effective fluid transport is controlled by the narrowest section of a pore which then determines the radius. [11]

For a typical porometry curve, see Figure 13. The Porolux software fills in Equation 5: the pressure and flow are measured and the surface tension of FC-43 is known to be 16.00 mN/m. This way, the bubble point, MFP and smallest pore size can be determined. Also, the pore size distribution is determined, for which more complex mathematical procedures are executed by the software (see Section 3.4.1).

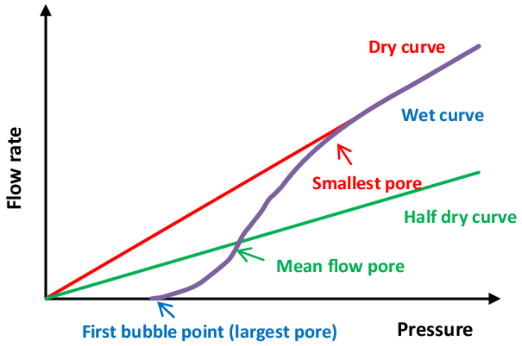

Figure 13: A typical (capillary flow) porometry curve. [20]

First, nitrogen is pushed through the membrane while it is still filled with the infusion liquid (FC-43), yielding the *wet curve*. The lowest pressure at which a flow is observed is called the first bubble point. Because the largest pores (or defects) are most easily opened, this pressure corresponds to the largest pore radius (r_p), since it requires the least pressure (ΔP) for nitrogen to permeate through the pore, in accordance with the Laplace equation. Then, the pressure and flow increase until all pores have been opened.

After that, the *dry curve* is measured, which should be linear because no pores are left to be opened; an increase in pressure should result in a proportional increase in flux. The point where the wet curve and the dry curve meet, contains the pressure at which all pores have been opened, including the smallest (and most "difficult" pores). Therefore, this intersection can be used to determine the smallest pore size.

Finally, the flow rates of the dry curve are divided by two, in order to obtain the intersection between the *half dry curve* and the wet curve. This intersection gives the pressure at which 50% of the gas flow can be accounted; the mean flow pore size (MFP). [21]

3.4 Liquid-liquid displacement porometry

Liquid-liquid displacement porometry (LLDP) is the main measurement technique in this research for learning more about SLIM stability. LLDP shows many similarities with GLDP as discussed in Section 3.3.2. For example, the SLIMs are liquid infused membranes that are tested by pushing an invading medium through them. In the case of LLDP however, the invading fluid is liquid (aqueous) instead of gaseous (nitrogen). Moreover, in this case the flux is kept constant and the required pressure is measured, as opposed to GLDP. A disadvantage of LLDP over GLDP is the long time required for reaching the desired liquid-liquid equilibrium. As mentioned in Section 3.3.2, this stability is needed to ensure that all pores of the same diameter are completely opened.

Setup

The setup used for the LLDP measurements consists of a liquid reservoir, a pressure meter, a flow meter/controller and a sample holder (Figure 14a). A keg made from stainless steel is used as the liquid reservoir, see Figure 14b. The system is pressurised to 4.5 bara by pushing nitrogen directly into the keg (at the top) after it is filled with the appropriate solution. The liquid contents are pushed to the flow controller (Bronkhorst mini CORI-FLOW™), then to the pressure meter (Bronkhorst IN-PRESS) and finally through the membrane. It is an important feature of the setup that the solutions are pushed from the bottom, because the top layer of solution in the keg tends to get saturated with the nitrogen, which is present at a high pressure. For this reason, a relatively large excess of solution is needed to prevent the nitrogen saturated top layer from entering the system during a measurement. The saturated nitrogen can form bubbles in e.g. the flow controller or the membrane, which can cause dewetting of the membrane and thus deviating results.

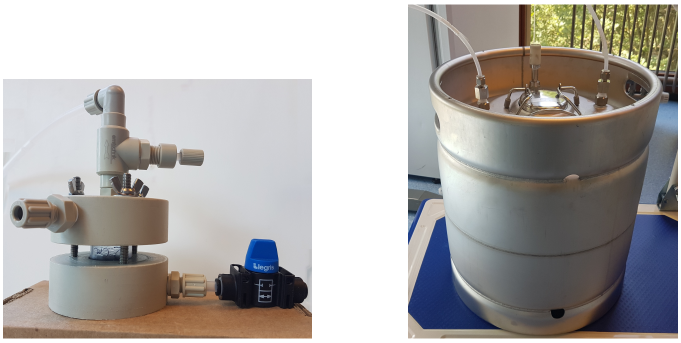

(a) The sample holder in the setup.

(b) The keg from stainless steel used as nitrogen pressurised liquid reservoir.

Degassing and cleaning
Before each measurement, any bubbles are pushed from the setup by pushing the contents of the liquid reservoir (water or surfactant solution) through the system and disposing it via the degassing tube (top of the sample holder shown in Figure 14a). Because bubbles would often form during this degassing, the flow is increased to values up to 70% for short periods until no more bubbles are formed. It is important to do this before every measurement, because gas bubbles can cause sudden increases of flow and affect measurements by dewetting parts of the membrane.
Before each new surfactant solution, the setup was cleaned by pushing nitrogen through the system for at least 15 minutes, then flushing the system with ≈ 10 L of water at increasing flows up to 70%.

Operation
The system operates flux-controlled: the PID control in the software tries to obtain a stable flow, while the pressure needed for this is measured. The flow values are later converted to fluxes using the membrane area. Bronkhorst software is used for controls and measurement.
For the dry and liquid infused membranes, a cyclic script is executed to measure a wide range of flows, see Table 3. The maximum flow (30 kg/h) determines the absolute flow values associated with the percentual values specified in the script. The maximum pressure of one of two calibration curves (up to 1.1 bar or 6 bar) determines the absolute pressure associated with the measured percentages. Because each run is executed twice, the differences in pressure can be observed between opening pores (first runs) and flow through pores already opened (second runs). For the newer membrane with smaller pore sizes (see Section 4.2), the pressure would sometimes increase to such extent that the flow controller could not reach the set flow value. For these measurements, the script shown in Table 3 was adapted to not exceed 50% flow. The prewet membranes were tested using two runs up to 70%, or 50% for the new membrane with the smaller pores.

Table 3: The script for the cyclic LLDP measurements. Each run is executed twice.

Run	Step size	Step duration
5%	1%	100 s
10%	1%	100 s
20%	2%	100 s
40%	5%	100 s
70%	10%	100 s

A Matlab script was written to quickly process measurements. This script takes the pressure average of the last few seconds of each step. The exact amount of seconds can be specified manually per run, based on the stability of a step. In the case of an unstable step, a smaller interval is taken. Additionally, the script makes a linear interpolation if points in the time array of the measurement are missing, due to the software sometimes omitting one or several data points. Also, a small script was written in Excel which can automatically switch between pressure calibration curves. For pressures above 1.1 bar, this ensures a switch is made to the 6 bar curve.

The pressure and flow values are subsequently processed into a pressure-flux plot. As these plots are sometimes difficult to interpret, especially for surfactant solutions, a clear example is shown in Figure 15 for a dry membrane with water. It can be seen that the first runs show a curved trend, whereas the second runs are linear or almost linear, because the pores that open at these pressures have already been opened. The blue line represents the prewet curve, which is again (almost completely) linear because the pores do not need opening due to the prewetting.

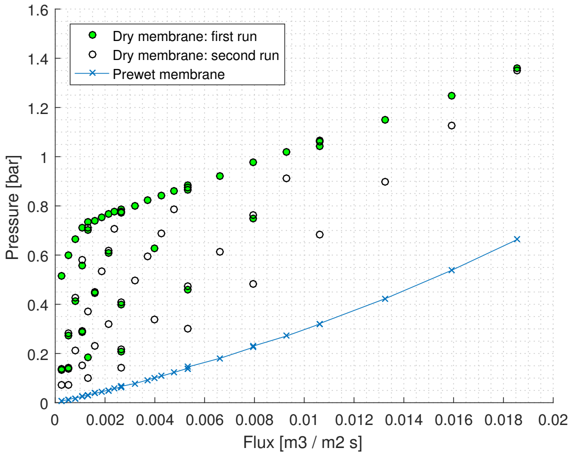

Figure 15: Cyclic LLDP measurement on dry membrane with water.

The results will be evaluated by comparing membranes (dry, Krytox infused or silicone oil infused) with each other per surfactant, and by comparing surfactants to each other per membrane type. Also, the results will be compared to theoretical predictions, using the Interfacial Pore Flow model (Section 3.4.1) and the Laplace equation (Section 2.1.2), which can be employed to predict critical pore opening pressures given pore sizes, (advancing) contact angles and surface/interfacial tension.

3.4.1 Interfacial Pore Flow model

The Interfacial Pore Flow model that is used in this research relates the actual membrane flux to the pressure, and is based on the Laplace equation. For describing the liquid transport, the model incorporates the Hagen-Poiseuille flow for convective liquid transport through cylindrical pores. Both models are described in Section 2.1.2. In practice, the simplification of the complicated membrane structure by assuming cylindrical pores is justified, because the liquid transport is governed by the narrowest pore sections ("pore-throats") with a certain radius. However, it should be noted that the assumption of this model still leads to a small deviation. [11]

There is an important complication in composing a model like this one. Each experimental flow value arises not only from the pores that are opened at a certain pressure, but also from larger pores (which have already been opened, for a large pore radius is associated with a lower critical pressure according to the Laplace equation). For this reason, the Hagen-Poiseuille equation (Equation 3) can not be applied directly. Instead, procedures of more mathematical complexity are needed that incorporate the pore size distribution, so that the contribution of each pore size is accounted for. The method used for this model was developed by Grabar and Nikitine. The approach for this model is to use the well-known log-normal pore size distribution (PSD), which is appropriate for many membranes. [11] A log-normal PSD means that the logarithm of the PSD is normally (or Gaussian) distributed.

The final result is the model shown in Equation 6. The advantage of this model is its physical basis: no polynomial fitting without physical meaning is performed, but fitting based on physical phenomena.
The upper limit of the integral (∞) is the radius of the biggest pore, while the lower limit (r) is the smallest pore size that is opened at the applied pressure ΔP. [11]

$$J(\Delta P) = \frac{N\pi\Delta P}{8\sqrt{2\pi}\ln(S)\eta l}\int_r^\infty r^3 exp\left[-\frac{1}{2}\left(\frac{\ln(r/R)}{\ln(S)}\right)^2\right]\mathrm{d}r \tag{6}$$

Furthermore, N is the total pore number density ($pore/m^2$), R is the geometric mean radius (m) and S (dimensionless) is the scale parameter (geometric standard deviation). Tortuosity is taken into account by S. All of these parameters are used for fitting experimental data to the model. It is also likely these values will vary in reality. After all, the effective pore density depends on how many pores are opened, and the mean radius may be affected by the thickness of liquid lining by the infusion liquid. In order to improve computational speed of the fitting (which is also very important in e.g. quality control [11]), initial guesses are assigned to the fitting parameters. For R, the 95% pore size is taken. This is the pore size for which 95% of the membrane pores are smaller [22]. For S, 1.2 is assumed and the initial guess for the total number of pores is 10^7 $pore/m^2$.

In Figure 16 a theoretical example is shown for pure water. The curve in the beginning characterises the pore size distribution of the membrane. A narrow PSD will result in a small pressure range at which new pores are opened, whereas a broad spectrum of pore sizes will cause a wide range of pressures before the dependency becomes linear.

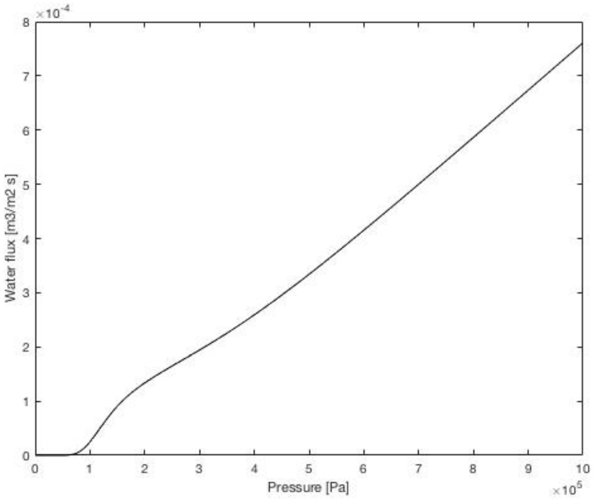

Figure 16: An example of a theoritcal Interfacial Pore Flow model curve.

3.5 Surfactant solutions

For making the surfactant solutions, first 1 to 2 L of concentrated solution is prepared by dissolving the total amount of surfactant needed for the final concentration. This was accomplished by intense magnetic stirring at water temperatures between 50 and 70 °C and leaving the stirring solution overnight. Finally, the solutions are placed in an ultrasonic bath for at least 30 minutes. The concentrated solutions are then diluted to 25 L (for 2 measurements) or 15 L (for 1 measurement). An excess of solution is needed because the top layer of liquid will tend to become saturated with the nitrogen present at 4 bara or higher, see Section 3.4. For the dilution, the keg is first filled with the required amount of pure water. Then the surfactant solution is added last to minimise bubbles, after which the diluted solution is stirred manually to ensure good mixing.

3.6 Microfluidic chip

In order to observe the displacement phenomenon, a hydrophobized microfluidic chip from BIOS is used together with a laser confocal scanning microscope (LCSM). Before use, the chip is cleaned by alternatingly flushing it with water and piranha acid (3:1 of sulphuric acid:hydrogen peroxide, volumetric), ending with water. After cleaning, the chip is hydrophobized with a coating of Trichloro(1H,1H,2H,2H-perfluorooctyl)silane (FOTS), by means of vapor deposition.
A confocal scanning microscope has the ability to capture a plane of focus while excluding as much light from other regions as possible. This results in very sharp images that would otherwise not be possible. [23]

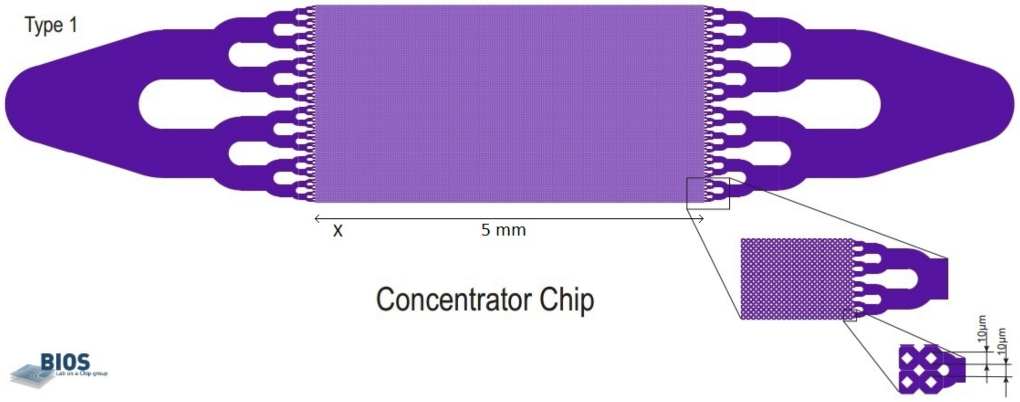

Figure 17: The microfluidic chip design by BIOS.

In Figure 17 the structure of the microfluidic chip is shown. The many inlets serve to ensure an equal distribution of incoming fluid.

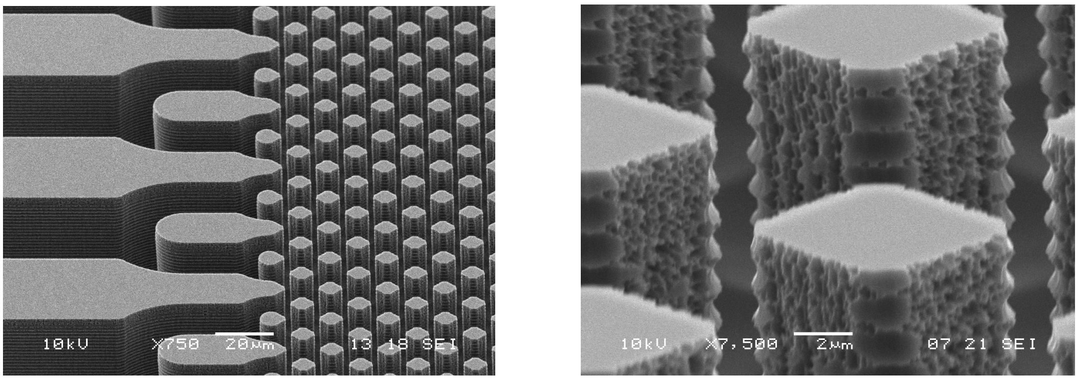

(a) Chip structure.

(b) Nanoroughness on the pillars of the chip.

Figure 18: SEM images of the microfluidic chip by BIOS.

In Figure 18, SEM images of the microfluidic chip are shown. In Figure 18b, the nanoroughness of the pillars can be observed, similar to the roughness observed with the PVDF membranes (Section 4.1).

The videos that are obtained from the microfluidic experiments are processed using an image analysis script in Matlab that calculates how much water is in the chip per time step. For this, the picture of the chip is sliced vertically into different sections. This yields S_{nw}, the saturation value of the non-wetting phase as a function of time and place in the chip. In this case the non-wetting phase is water (or a surfactant solution), because the surface is hydrophobic. Finally, the average degree of saturation is determined for each time step by combining all slices.

Temporal resolution

Nota bene: the size of one time step depends on the area that the microscope should capture. If only the part of the microfluidic chip with the pillars needs to be taken into account (instead of the full chip), each scanning streak of the microscope is shorter and therefore faster. Another upside to this is that just two pictures need to be merged, resulting in only one area of slightly lower image quality. For images of the full chip, four pictures are merged. This results in two areas of slightly lower quality and a lower temporal resolution (2 seconds per picture). However, the advantage of full scanning is the information about both sides (inlet and outlet) of the microfluidic chip.

3.7 Measuring SFT and IFT

The surface and interfacial tension (SFT and IFT) can be measured in several ways. The surface tension of all surfactant solutions are measured using the pendant drop method. Also, the interfacial tensions of all oil-surfactant solution systems are measured using pendant drop method.

Pendant drop method
Pendant drops are drops hanging from a flat, solid surface. [4] Pendant drops are affected both by gravity and surface tension. While surface tension results in a tendency to minimise the surface area (i.e. forming a perfectly spherical droplet), gravity pulls the droplet down and causes elongation. [24] If the densities of a pendant drop and its surrounding medium are known, the shape of a pendant drop hanging from a needle can be analysed optically. For a pendant drop at mechanical equilibrium, the forces are balanced. A numerical fit is then made to calculate the surface tension that causes the observed shape. Similarly, pendant drops can also be used for measuring interfacial tensions of liquid-liquid systems. In this case, a droplet of the heavy phase needs to be dispensed into the lighter phase. Otherwise, the drop will rise, making accurate measurements impossible.

The needle used to dispense the droplets is usually taken as a scaling reference. Scaling is necessary to determine the exact contribution of gravity to the droplet's shape. Furthermore, because the curvature of pendant drops is analysed, there should be a sufficiently large density difference between the two phases to allow for enough droplet elongation. In the case of very similar densities, droplets will take on a very spherical shape which does not allow for realistisc measurements.
This problem occurrs with silicone oil in water due to the small density difference. For this reason, the interfacial tensions for the silicone oil systems are also measured using the Wilhelmy plate method.

Wilhelmy plate
Surface and interfacial tensions can also be measured using the Wilhelmy plate method. This method makes use of a flat plate that can be perfectly wetted by the liquid. [4] After immersion into the liquid, the plate is lifted a bit out of the fluid to measure the amount of force needed for this, as is shown in Figure 19. The surface tension of the fluid acts along the line of contact with the plate, equal to $2(w + d)$. The only correction the Wilhelmy plate method needs is taking into account the buoyancy of the plate [4].

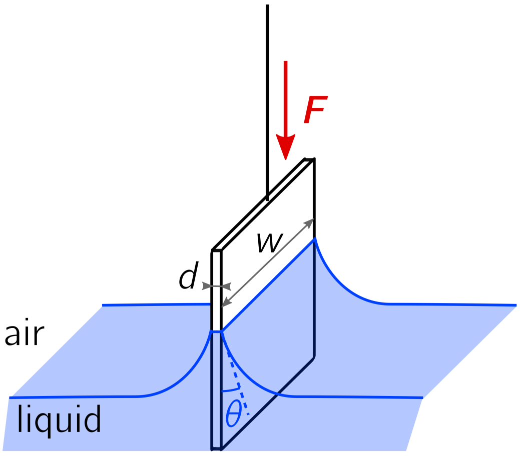

Figure 19: A Wilhelmy plate immersed in a liquid. [25]

Similar to the pendant drop method, the Wilhelmy plate can also be employed for measuring interfacial tensions. In this case, the procedure consists of three steps. First, the light phase is measured for taring. Secondly, the light phase is replaced with the heavy phase and the surface is detected by the measuring machine. Thirdly, the light phase is added carefully on top of the heavy phase and the interfacial tension is measured. A requirement for interfacial wilhelmy measurements is a horizontal interface. Between measurements, the Wilhelmi plate can be cleaned with a burner.

Nota bene:
Due to equipment software not being up to date, all SFT and IFT measurements described above were performed at Wetsus, Leeuwarden.

3.8 Contact Angle (Hysteresis)

Contact angle measurements are performed for information about the advancing contact angle of surfactant solutions in the dry membrane. The contact angles are measured by dispensing a droplet on a flat, solid surface (a sessile droplet). The dispensing needle stays within the droplet and alternates increasing and decreasing the droplet volume continuously. The initial droplet volume is 2 μL, which is increased to 6 μL at 0.5 $\mu L/min$ in six cycles. There is a 2 second delay between each advancing and receding measurement. The contact angles are measured with image analysis software.

The surface should represent the conditions encountered in the membrane pores. This means that the regular porous membrane cannot be used for these measurements, but instead a dense membrane should be used to mimic the pore walls.

4 Results and Discussion

Different membrane sheets

During this research, different membrane sheets were used for the porometry measurements. The sheet that was used for most of the measurements, is the one made on 10-01-2017 (membrane I) with a dope solution that was about a year old at that time.

Because there was not enough left of this membrane to finish all the measurements, a new membrane was fabricated on 21-04-2017 (membrane II) using a fresh dope solution. However, it was observed with gas flow porometry that this new membrane was significantly more dense than the previous one, see Section 3.3.2. This resulted in higher pressures which was sometimes problematic for the L-L displacement setup, which is limited by the pressure meter (< 6 bar). On 08-06-2017 (membrane III), it was attempted to reproduce membrane I using a longer coagulation time (60 minutes instead of 30), in order to allow for more coagulation. However, the fabricated membrane showed the same pore sizes as membrane II.

4.1 SEM

4.1.1 Membrane I

The SEM results of membrane I (10-01-2017) are shown in Figure 20.

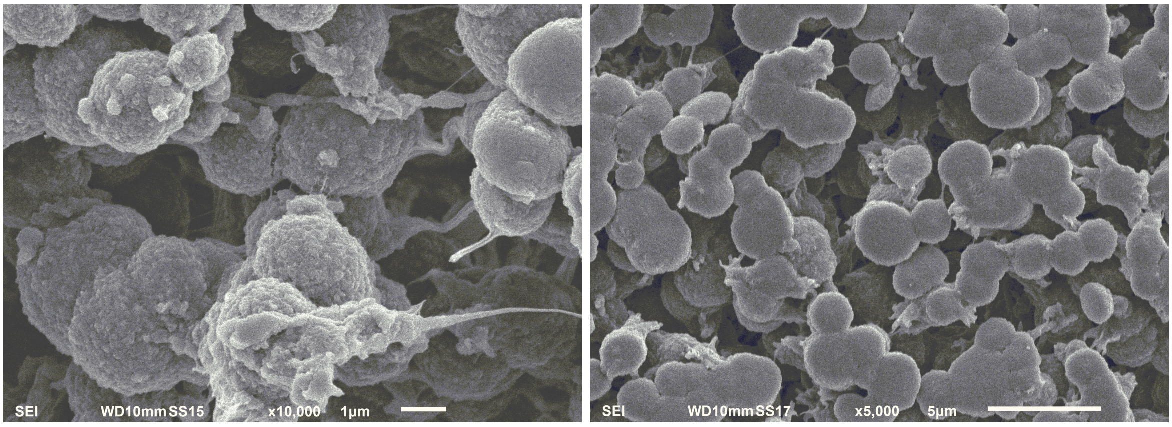

(a) Top, 5000x magnified.

(b) Bottom, 5000x magnified.

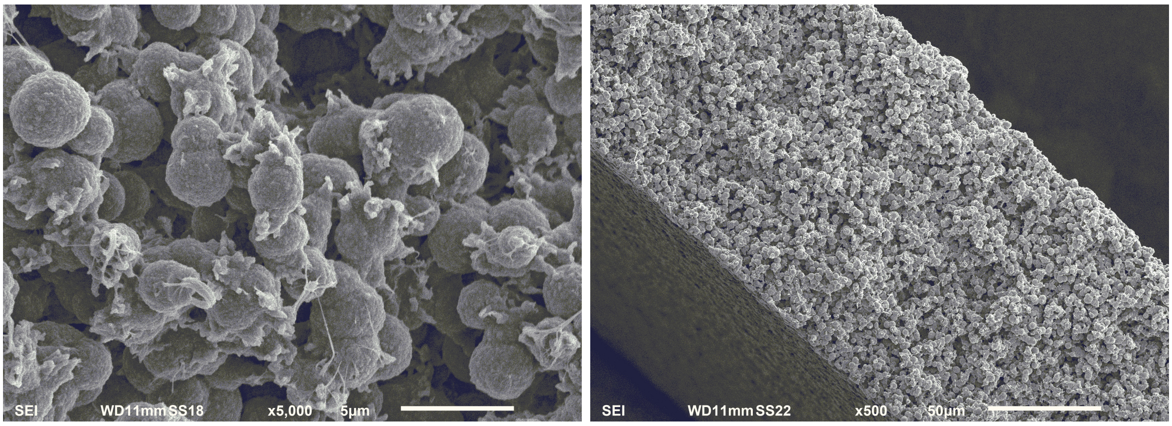

(c) Cross section, 5000x magnified.

(d) Cross section, 500x magnified.

Figure 20: SEM images of PVDF membrane I (made on 10-01-2017).

The difference between the top and the bottom of the membrane is clearly visible in Figure 20a and Figure 20b. For the top, the PVDF particles take on a spherical shape, whereas the bottom shows a top layer of flattened PVDF particles, due to contact with the glass plate. The roughness on the PVDF particles can be observed. Also the membrane thickness can be estimated, using the scale (50 μm) provided by the SEM: $\approx 130\ \mu m$.

4.1.2 Membrane II

The SEM results of membrane II (21-04-2017) are shown in Figure 21.

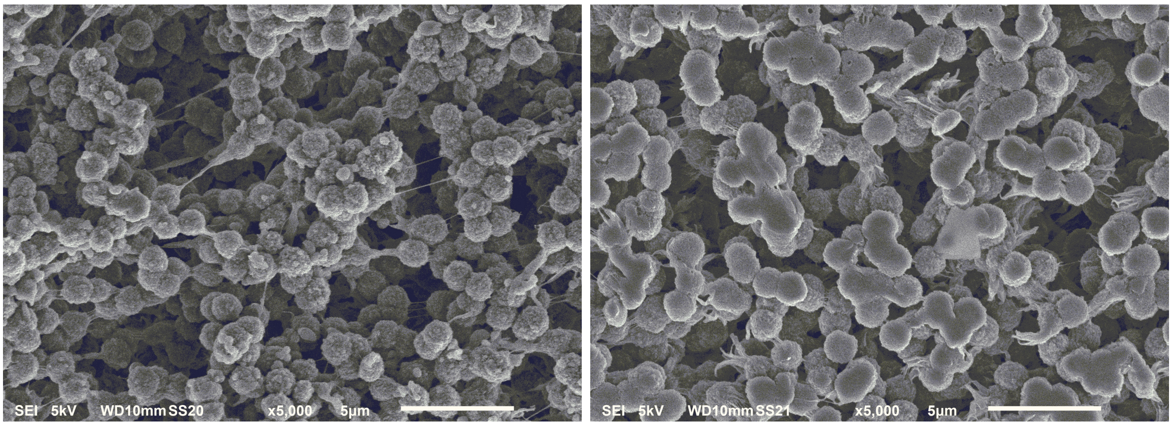

(a) Top, 5000x magnified.

(b) Bottom, 5000x magnified.

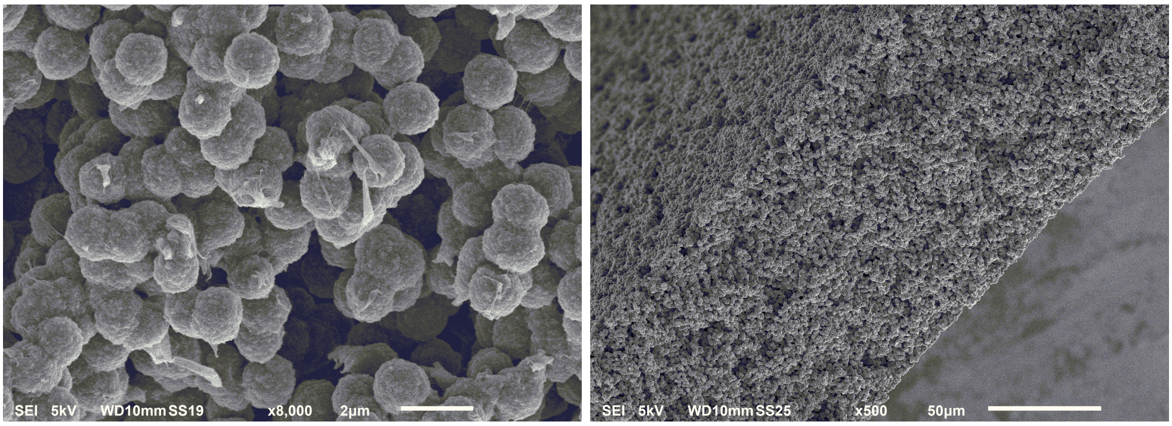

(c) Cross section, 8000x magnified.

(d) Cross section, 500x magnified.

Figure 21: SEM images of PVDF II membrane (made on 21-04-2017).

From Figure 21d the membrane thickness can be estimated, using the scale (50 μm) provided by the SEM. The measured thickness is $\approx$ 111 μm. Again, a clear difference between the top and bottom structure of the membrane is observed, as well as surface roughness.

4.2 Gas-liquid displacement porometry

Below are the capillary flow porometry results for membranes I, II and III, see Table 4.

Table 4: GLDP results (diameter)

Membrane	95% pore size	MFP size	Bubble point pore size	Smallest pore size
I	2.161 μm	2.514 μm	2.586 μm	1.860 μm
II	1.323 μm	1.468 μm	1.517 μm	1.102 μm
III	1.261 μm	1.446 μm	1.475 μm	1.026 μm

It was surprising that membrane III exhibits pore sizes even smaller than membrane II, despite the coagulation time being twice as long for the III membrane (60 minutes versus 30 minutes). This suggests that the influence of coagulation time on the membrane structure is very limited. Most likely, the age of the dope solution has a larger influence, possibly due to the NMP contents slowly evaporating over time.

4.3 SFT & IFT measurements

Surface tension
The SFT measurement results are shown in Table 5. The SFT results (pendant drop method) are shown in Table 5. As an example, one of the analysed pictures is shown in Figure 22a.

Table 5: Surface tension values from pendant drop method.

Solution	Surface tension [mN/m]
MQ	67.67
SDS	62.61
CTAB	32.66
Triton	31.83
DDAPS	36.74

The IFT results are shown in Table 6. Note that oil droplets were submerged in the aqueous phase because of their larger density. Performing the measurement the other way around would result in inaccurate measurements and rising bubbles. A nice example of a Krytox droplet in water is shown in Figure 22b.
The error in image analysis techniques for measuring surface and interfacial tensions can be quite large. A difference in illumination, focus or magnification can already cause deviations, as was observed with water (Table 5). Several attempts were made to obtain the expected value of 72 mN/m, but without success. During the second visit at Wetsus, the magnification was altered and the measured SFT for pure water was 72 mN/m, as expected. However, there was no time to redo all experiments so the values shown in Table 5 are used while keeping in mind that the actual value might be slightly larger, as with water. For water, 72 mN/m will be used.

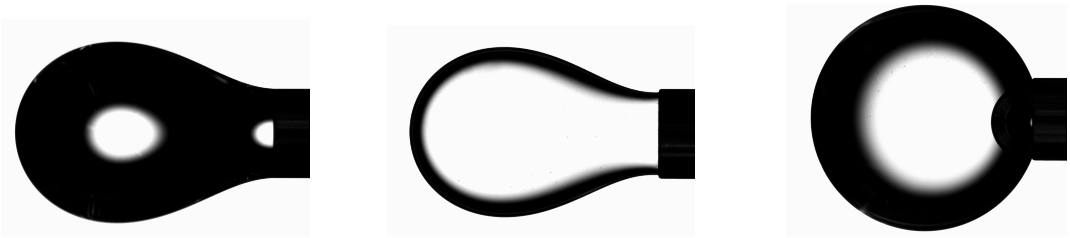

(a) Pendant drop of surfactant solution in air.

(b) Pendant drop of Krytox 101 in a surfactant solution.

(c) Pendant drop of SO AR20 in a surfactant solution.

Figure 22: Pictures of the pendant drop method for different systems.

Interfacial tension (pendant drop)
The IFT measurement results from pendant drop method are shown in Table 6. It is important to note that the values for silicone oil are considered highly unreliable due to the minimal difference in density between water and silicone oil. This caused very spherical droplet shapes, which does not allow for an accurate calculation of the IFT because of the curvature. An example is shown in Figure 22c. Still, the measurements were finished because the image analysis software could register differences in curvature and thus calculate different IFT values. If anything, these pendant drop IFT values for silicone oil are only suitable for roughly comparing silicone oil systems with each other, but they should not be considered realistic on their own.
Moreover, a more reliable Krytox measurement in water revealed an IFT of 54 mN/m, instead of 48.55 as shown in Table 6. The value of 54 mN/m is assumed.

Table 6: Interfacial tension values from pendant drop method.

Solution	Oil	Interfacial tension [mN/m]
MQ	Krytox 101	48.55
	SO - AR20	60.94
SDS	Krytox 101	37.58
	SO - AR20	59.93
CTAB	Krytox 101	16.81
	SO - AR20	8.65
Triton X100	Krytox 101	11.87
	SO - AR20	38.87
DDAPS	Krytox 101	16.70
	SO - AR20	4.95

Interfacial tension (Wilhelmy plate)
Due to the unreliable IFT results for silicone oil with the pendant drop method, the Wilhelmy plate was employed

as well. However, it has proven quite difficult to obtain a stable, horizontal interface of water and silicone oil. The first attempt resulted in a vertical interface, see Figure 23 (left).

Figure 23: The interfaces obtained with a system of silicone with pure water (left) and salty water (right).

Later, salt (pure NaCl) was added to increase the water density and thus the density difference with silicone oil. It was observed that water became the denser phase and after adding ≈ 1 g of salt, a horizontal interface was obtained (with silicone oil on top). As the Wilhelmy plate can also be used for a swift SFT measurement, the salty water solution was measured before oil was added. For pure water, 71.2 mN/m was measured, but for the salty solution values around 57 mN/m were measured. It is believed this difference is too large to be caused by the addition of salt, and the deviation is an error caused by another external factor, e.g. contamination with silicone oil despite good cleaning.
Due to a shortage in time, the IFT values for silicone oil in surfactant solutions could not be finished, so a small experiment was conducted to observe how the presence of SDS molecules would affect the oil-water interface. Similar to the formation of emulsions, silicone oil droplets were presumably stabilised by the presence of the surfactant. This is shown in Figure 24, where it can be seen that two droplets of silicone oil are very close, but no coalescence occurs. This is in agreement with expectations regarding emulsion stabilising abilities of surfactants, as is mentioned in Section 2.1.3.

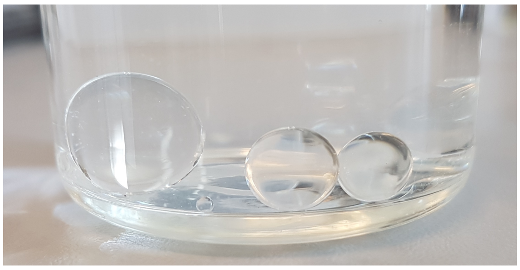

Figure 24: Droplets of silicone oil are stabilised by the presence of surfactant (SDS).

It is believed that the Wilhelmy plate cannot be a solution for reliably measuring systems consisting of silicone oil and surfactant solutions. First, without the addition of salt the density difference is too small to allow for a horizontal interface. It could be possible if water is added very carefully, but even then the interface is highly unstable and is likely to be disrupted by the plate, resulting in unreliable values. This problem will probably be aggravated by the presence of surfactants, which can result in droplets and no interface at all.
Second, it was observed that salt can help with obtaining a stable interface, but this would significantly increase the complexity of the system by interactions with the surfactants, resulting again in unreliable measurements.

After consultation within the SFI group, the interfacial tension for silicone oil with pure water is estimated at 25.5 mN/m. [26] Unfortunately, the values for silicone oil with surfactant solutions are not known yet.

4.4 Liquid-liquid displacement porosimetry

Prewetting
The LLDP measurements shown in Figure 25, 26, 27 and 28 are performed on membrane I. The prewet curves shown for comparison in these figures originate from membranes that were prewet with pure water. Prewettting

was achieved by first infusing with ethanol, as described in Section 3.2.3. Later, it became clear that prewetting with the appropriate surfactant solution would be better for a fair comparison. However, because this membrane was finished, these surfactant prewet measurements were performed on the denser membrane II. Unfortunately, the pores of this membrane are significantly smaller (resulting in higher pressures), which makes it impossible to make a good comparison between the surfactant prewet, the regular prewet and the other membranes.

Still, it can be argued that prewetting with pure water instead of the appropriate surfactant solution - while not completely adequate - does not produce any problems for the discussion of the results below. After prewetting with water, the membrane is completely filled with pure water instead of surfactant solution. During LLDP measurements, this may result in a gradient of surfactant concentration, resulting in Marangoni flow into the membrane (Section 2.1.3) and lower pressures. But the Marangoni effect is generally very small, especially for the small amount of infused water which will be readily replaced by the surfactant solutions. Therefore, the observation that the prewet pressurse never exceed the pressures of the dry membranes and SLIMs (which supports the notion that there is still infusion liquid left) is deemed correct, despite "wrong" prewetting.

Because of membrane I being finished, the DDAPS (zwitterionic) measurements shown in Figure 29 were performed on the denser membrane II, resulting in higher pressures overall. Still, the DDAPS measurements can be compared to each other. The membranes for the prewet DDAPS curves were prewet with the surfactant solution and not with water.

Pressure buildup
For some of the measurements, a pressure buildup between runs is observed to a greater or lesser extent. The second runs can exhibit higher pressures than first runs, which is not expected because more pores should be open in the second runs than in (the beginning of) the first runs.
The first explanation that comes to mind is the system not yet being at equilibrium. The raw (non-analysed) pressure data confirms this; the runs up to 40% and 70% in particular often show a deviation from the desired stable pressure plateau to analyse. However, pressure buildups are observed for both kinds of pressure instability: sometimes the pressure is still increasing after 100 s, sometimes the pressure is still dropping. In the last case, the pressure course often resembles the valley of a quadratic function. As was mentioned in Section 3.4, unstable pressure plateaus are analysed over a smaller time interval to obtain an average value closer to equilibrium. The fact remains that the buildup of pressures cannot be explained by instability alone.

Another plausible explanation is then accumulation of undissolved surfactant, resulting in clogging pores and higher pressures. Special care has been taken to maximise surfactant dissolving, but without a surfactant dispenser complete dissolving cannot be guaranteed. While fouling by undissolved surfactant might be possible, there are also counter arguments. After magnetic stirring for many hours at high temperatures, the amount of undissolved surfactant is most likely very small. Also, no layer of surfactant was visible on the membrane surfaces after any of the measurements. An explanation related to the previous one is the formation of emulsions. Due to surfactant molecules forming micro-emulsions between surfactant solution and oil (Section 2.1.3), pores could get blocked.

It is also possible that surfactants are sticking to the membrane wall despite the protective liquid lining (adhesion). This can increase pressure by means of Marangoni stress, by the repelling tendency of new surfactant molecules with adhered surfactant molecules with the same charge, or a combination of both.

In brief, it is not yet certain what is the exact cause of the pressure buildup, so more research would be needed to disclose its origin. If accumulation of surfactants indeed occurs despite liquid lining of the pores, this could be a serious problem for the anti-fouling properties of SLIMs.
It could also be a problem for reliable measurements, if the pressure increasing effects are responsible for the SLIM pressures being higher than the prewet ones instead of the liquid lining. However, it is highly unlikely that surfactant adhesion or fouling only occurs for SLIMs and not for prewet membranes. Still, emulsion formation is something that would likely increase pressures and can only occur in SLIMs, so future research would have to rule this out.

4.4.1 Infusion liquids compared

Below are the LLDP results shown per surfactant (pure water, SDS, CTAB, Triton X100, DDAPS). The full figures can be found in the appendix, Section 7.1.

It can be observed for the different surfactant solutions (and MQ) that silicone oil infused membranes are fairly consistent in showing unexpected first runs, more specifically the 5% and 10% first runs (up to 0.0025 m^3/m^2s).

Arguably, the cause for this is the small density difference between water and silicone oil. This can result in unexpected behaviour like unstable interfaces and droplet formation (especially for surfactant solutions), as was observed with interfacial tension measurements (Section 4.3). The behaviour of Krytox oil is more in line with expectations.

Pure water

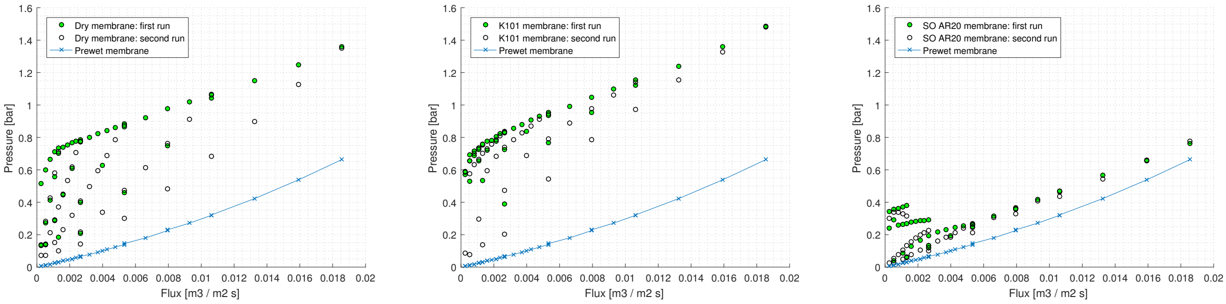

(a) Dry membrane with MQ.

(b) Krytox 101 infused membrane with MQ.

(c) Silicone oil AR20 infused membrane with MQ.

Figure 25: The analysed LLDP results for pure water (MQ).

When considering the opening of pores according to the Laplace equation (Equation 5), perfect wetting of the wall can be assumed for both infusion liquids. This is because the immiscible liquid-liquid contact of the infusion liquids with water results in a liquid interface, meaning perfect wetting is achieved. In addition, the infusion liquids show spontaneous wicking into the membrane, ensuring complete wetting of the membrane by the oils. Because of perfect wetting, any observed pressure difference arises from a difference in interfacial tension, a difference in pore radius (by liquid lining) or a combination of both.

The SFT for MQ in water is 72 mN/m (Section 4.3) and the advancing contact angle of water on a dense membrane is equal to 122° (see 3.8), resulting in the following effective surface tension: $\gamma \cdot |\cos\theta| = 72\ \text{mN/m} \cdot |\cos 122°| = 38.15\ \text{mN/m}$. The IFT of Krytox 101 with water was measured to be 54 mN/m (Section 4.3). The IFT of silicone oil is taken to be 25.5 mN/m (Section 4.3).

These values correspond with the observed pressures shown in Figure 25. The highest pressures are observed for the Krytox 101 infused membrane, while the SO AR20 infused membrane shows the lowest pressures. The SLIM pressures are consistently higher than the prewet pressures. If all of the infusion oil were to be removed by the water, it would be expected that the SLIM pressures would converge to those of the prewet membranes. After all, if the oil has been replaced by water, the SLIM is identical to a prewet membrane. However, higher SLIM pressure than prewet pressures are observed for both SLIMs, suggesting that there is oil remaining on the wall up until the highest flux values. Furthermore, the clear difference between the dry membrane and the SLIMs implies a difference in wetting: partial wetting for the dry membrane and perfect wetting with infusion liquids for the SLIMs. This again supports the notion that there is still infusion liquid present in the SLIMs.

Sodium dodecyl sulfate (SDS)

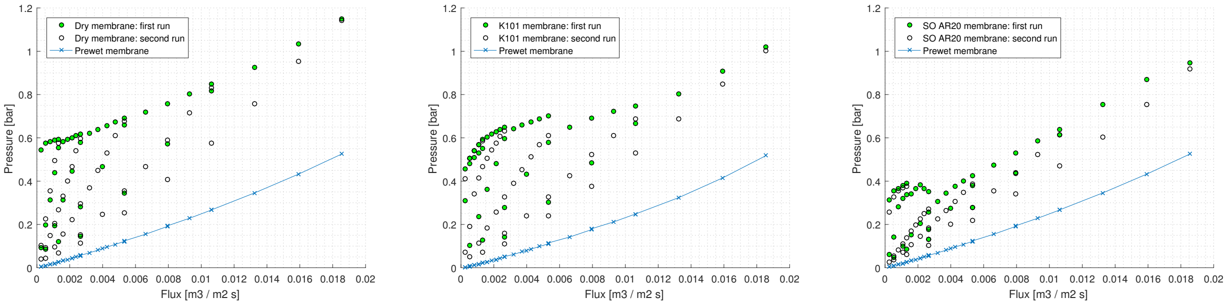

(a) Dry membrane with SDS solution.

(b) Krytox 101 infused membrane with SDS solution.

(c) Silicone oil AR20 infused membrane with SDS solution.

Figure 26: The analysed LLDP results for SDS (anionic).

The SFT value for SDS in air is 62.61 mN/m. The IFT value of SDS with Krytox was measured to be 37.58 mN/m. For silicone oil, no reliable value is known but it is assumed that the interfacial tension will be lower than 25.5 mN/m (IFT of silicone oil with pure water) due to the presence of surfactants. Interfacial tensions of systems with Krytox and surfactant solutions were always lower than for pure water.
When calculating the effective surface tension of SDS solution in air, the advancing contact angle needs to be taken into account. However, as the contact angle measurements on the SDS solution were not successful, no reliable value is known (Section 4.7). Still, the pressure ratio between Krytox/dry membrane (≈ 1 at the initial fluxes) would suggest an advancing contact angle of 127°, which is relatively close to the observed value of around 111°, although this value is not reliable.

Again, the pressures are always higher than the prewet measurement, suggesting oil is still present in the SLIMs even at the higher fluxes. It is difficult to make a comparison between the dry membrane and the SLIMs, as the advancing contact angle and silicone oil IFT are unknown. However, there is agreement between theory and practice for Krytox and silicone oil, particularly when looking at the pressures for the first two or three runs. Lower pressures are indeed expected for silicone oil, which exhibits a lower interfacial tension with SDS solution than Krytox.

Cetyl trimethylammonium bromide (CTAB)

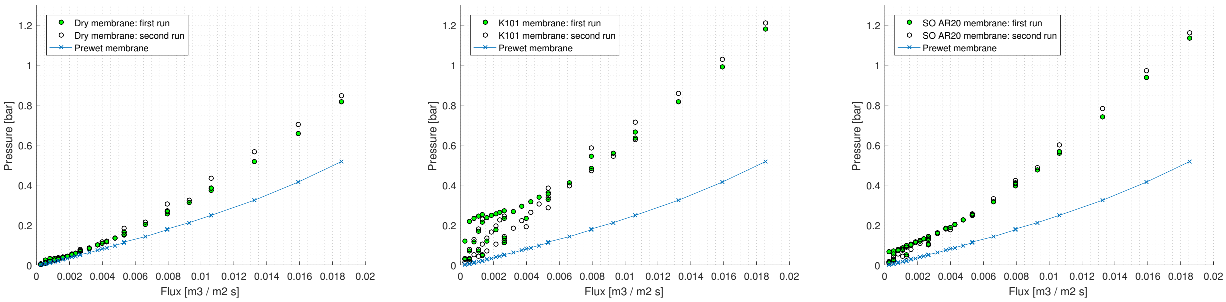

(a) Dry membrane with CTAB solution.

(b) Krytox 101 infused membrane with CTAB solution.

(c) Silicone oil AR20 infused membrane with CTAB solution.

Figure 27: The analysed LLDP results for CTAB (cationic).

The contact angle of CTAB solution is not known and the interfacial tension of silicone oil with CTAB solution should be somewhere below 25.5 mN/m. The surface tension of CTAB solution in air is 32.66 mN/m, but the effective surface tension cannot be determined without knowing the contact angle. A rough estimation would be to assume an advancing contact angle of 110 ° again, which would result in $\gamma = 11.17\ mN/m$ and correspond with the observation of lower pressures than the Krytox infused membrane. The interfacial tension of CTAB with Krytox is 16.81 mN/m.

The results suggest that there's a pressure build-up between runs for all three membrane types. The cause of this can be one (or a combination) of the phenomena as discussed in the beginning of this section: the formation of emulsions, surfactant adhesion or accumulation of undissolved surfactant. Because CTAB has proven very difficult to dissolve (temperatures of 50 °C were required before any significant dissolving occurred), clogging of membrane pores is a plausible explanation.

As with the previous surfactant solutions, the difference with the prewet curves indicate the presence of infusion liquids up to the highest fluxes. Furthermore, the difference between first and second runs for Krytox strongly suggests pores are being opened, implying liquid lining. For silicone oil, this is observed to a lesser extent. This could be due to a lower interfacial tension, but in the case of a significant IFT difference with respect to Krytox this would most likely present itself by much lower pressures overall, while it is only observed in the beginning. In the case of fouling of course, it could still be a possibility that the silicone oil pressures are inherently lower but are increased by clogging pores or emulsions. Possibly, it is the result of the small density difference causing unexpected behaviour.

Triton X100

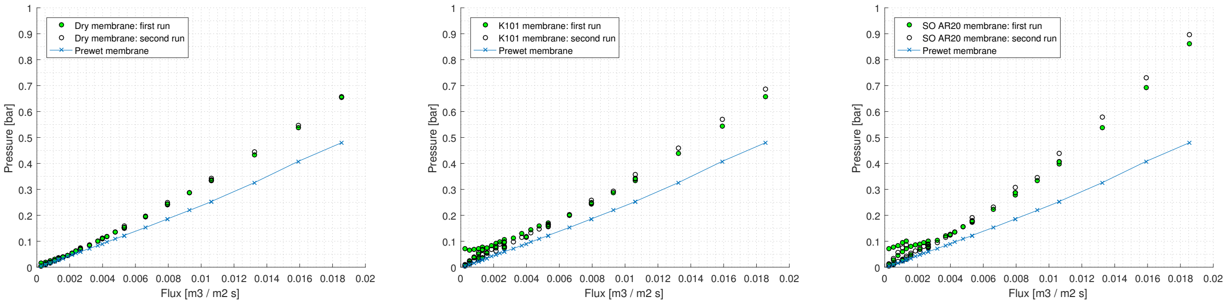

(a) Dry membrane with Triton X100 solution.

(b) Krytox 101 infused membrane with Triton X100.

(c) Silicone oil AR20 infused membrane with Triton X100.

Figure 28: The analysed LLDP results for Triton X100 (non-ionic).

The surface tension of Triton X100 solution in air amounts to 31.83 mN/m, but the effective surface tension will be significantly lower due to the advancing contact angle. This is most likely the reason for the small difference between the dry membrane and Krytox. The interfacial tension of Krytox is 11.87 mN/m. The interfacial tension of silicone oil should be somewhere below 25.5 mN/m.

A small difference is observed between the pressures of the prewet curve and the SLIMs. This can be explained: the interfacial tension of Krytox in Triton solution is the smallest one. The dry membrane also shows pressures very similar to the prewet membrane. The pressure difference for SLIMs with respect to prewet, together with a (small) difference between first and second runs, indicate the presence of infusion liquid.

N-Dodecyl-N,N-dimethyl-3-ammonio-1-propanesulfonate (DDAPS)

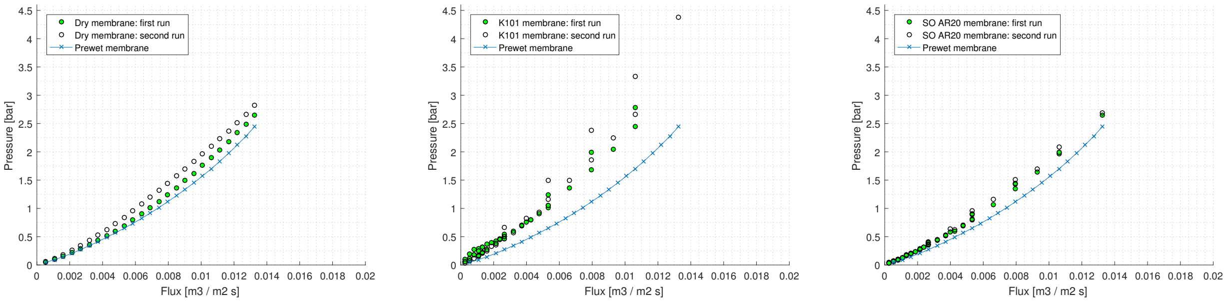

(a) Dry membrane with DDAPS solution.

(b) Krytox 101 infused membrane with DDAPS solution.

(c) Silicone oil AR20 infused membrane with DDAPS.

Figure 29: The analysed LLDP results for DDAPS (zwitterionic).

The surface tension of DDAPS solution in air is equal to 36.74 mN/m, but will effectively be reduced by the advancing contact angle. The interfacial tension of DDAPS solution with Krytox is 16.70 mN/m. Silicone oil will again result in values below 25.5 mN/m. The dry measurement was unintentionally performed with the non-cyclic script, but because it was very similar to the prewet measurement (likely due to a very small effective surface tension), this is not deemed problematic. Also, it can be seen that the higher fluxes are not reached for these measurements while the pressures are much higher than for the other surfactant solutions. As mentioned before (and shown in Section 4.2), DDAPS was tested on membrane II, which exhibits much smaller pore sizes. Physical limitations of the setup prevented measuring fluxes for which pressures higher than ≈ 4 bar are needed.

Nonetheless, the DDAPS results allow for some interpretation. A pressure difference exists between the SLIM curves and the prewet curves (prepared with the surfactant solution for DDAPS), suggesting the presence of infusion liquid. For the SLIMs, the first and second runs are very similar for the lower fluxes. This effect is stronger for silicone oil than for Krytox, which still shows some difference. However, the difference with prewet is so small for silicone oil that much of the oil is probably removed, as the pressures converge to those of the prewet membrane. The measurements with the microfluidic chip confirm this notion (Section 4.6).

4.4.2 Surfactants compared

When looking at the different surfactants per membrane type (dry, Krytox infused or silicone oil infused), a rough comparison can be made. The DDAPS solutions are left out of the comparisons because of the strongly different membrane.

Dry membrane
For the dry membrane, the SDS solution causes the highest overall pressure compared to the prewet membrane. Slightly lower pressures are observed for CTAB, while the lowest pressures occur with the Triton solutions. This would suggest Triton readily removes oil from the membrane, while both CTAB and SDS are less harsh at these concentrations.

Krytox 101 infused membrane
For the Krytox membrane, SDS and CTAB show very similar pressures for the high fluxes when comparing their differences with the respective prewet curves. For the lower fluxes, SDS causes higher pressures. Also the second final runs (70%) show a large difference with the prewet curves, suggesting a respectable amount of oil is left in the membrane for both CTAB and SDS. Triton again present the lowest pressures with respect to the prewet curve, likely due to much oil being washed away.

Silicone oil AR20 infused membrane
The silicone oil membrane is the only type where higher pressures are obtained for a surfactant solution (CTAB) than with pure water. This could be due to the formation of emulsions and the small density difference with water. It could also be fouling by undissolved CTAB. SDS and CTAB are similar, although SDS (like with Krytox) shows a much larger difference between first and second runs, in particular for the lower fluxes. For Triton, the final pressure is significantly lower but the respective difference with the prewet curve is similar, suggesting the lower pressures are mostly caused by a low interfacial tension.

In conclusion, it seems Triton X100 (a non-ionic surfactant) is the most harsh surfactant in terms of oil removal, when looking at the LLDP measurements.

4.4.3 Interfacial Pore Flow model

The experimental data is fitted to the Interfacial Pore Flow (IPF) model, as described in Section 3.4.1.

The data that is used for the IPF model is generally taken from the first runs, because these hold information about the opening of the pores. However, sometimes a measurement series shows deviations in a first run, which makes it very difficult to obtain a good fit of the data to the model. For example, silicone oil measurements yield unexpected results sometimes, as described in Section 4.4.1. See also Figure 25c. In these cases, measurement points are extracted from the data that do allow for fitting with the model.

In Figure 30, the results are shown. Unfortunately, not all of the measurement data could be properly fitted to the model. Presumably, the cause for this is the deviating shape of some of the results, caused by kinetic phenomena in the membrane.
The water measurements were easily fitted. The closest fits are obtained for the dry and Krytox infused membrane, which is in agreement with observations of unexpected silicone oil behaviour.
On the other hand, silicone oil yields the closest fit for the SDS measurements. Here, the dry and Krytox infused membrane show larger deviations, especially at the lower pressures.
No close fit could be found for the dry membrane with CTAB solution. The silicone oil and Krytox infused membrane show nice fitting.
Finally, for Triton X100, a reasonable fitting could only be achieved for the Krytox infused membrane.

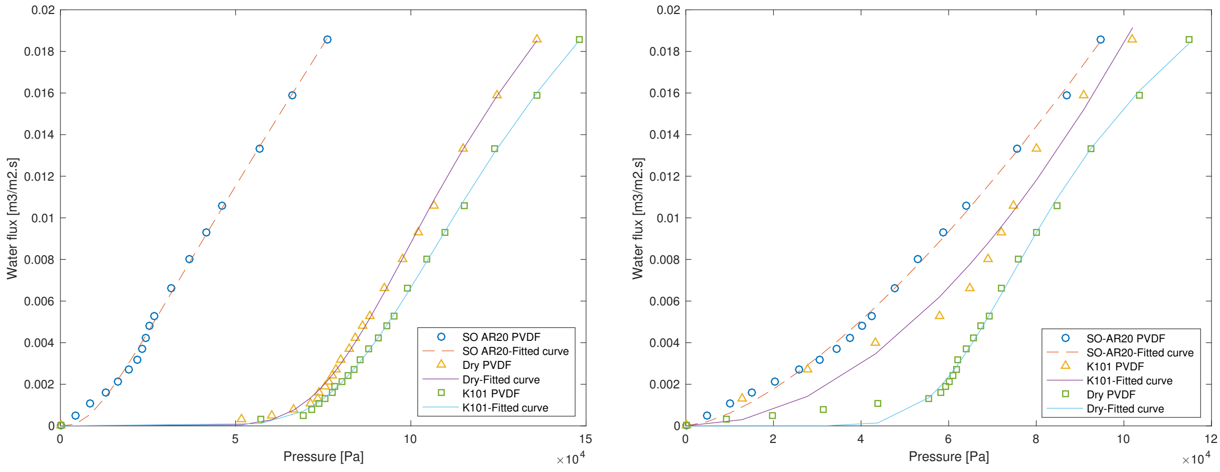

(a) Fitted LLDP results for MQ (ultrafiltrated water) through a dry and liquid infused membranes.

(b) Fitted LLDP results for SDS (anionic surfactant) through a dry and liquid infused membranes.

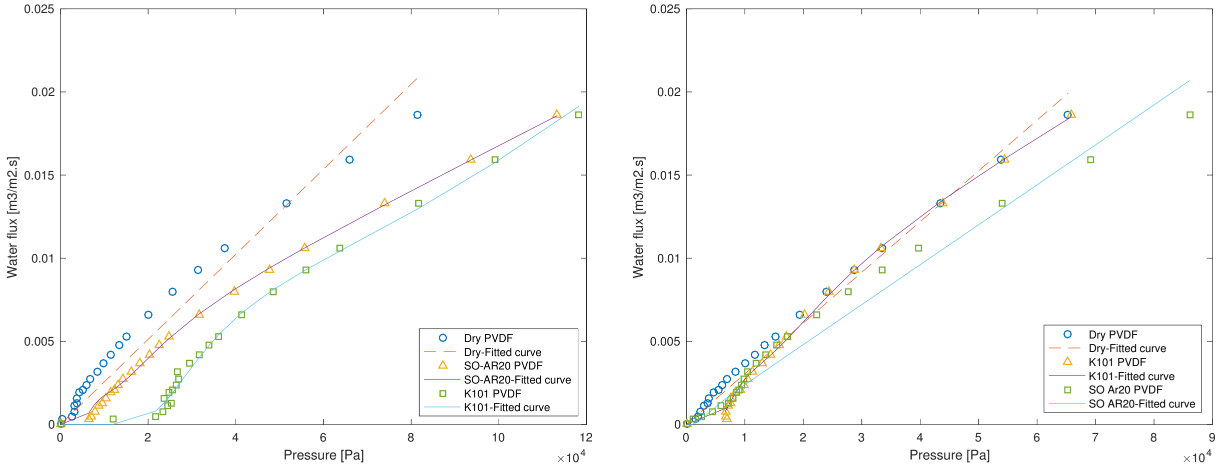

(c) Fitted LLDP results for CTAB (cationic surfactant) through a dry and liquid infused membranes.

(d) Fitted LLDP results for Triton X100 (non-ionic surfactant) through a dry and liquid infused membranes.

Figure 30: Fitted results for pure water and different surfactant solutions.

Because the different fitting results for Triton are very close to each other, they are presented separately in Figure 31.

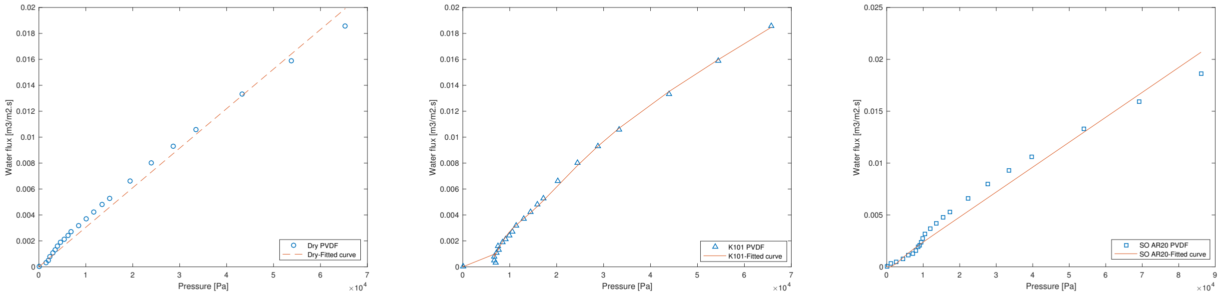

(a) Fitted LLDP results for the dry membrane.

(b) Fitted LLDP results for the Krytox 101 infused membrane.

(c) Fitted LLDP results for the silicone oil AR20 infused membrane.

Figure 31: Fitted results for Triton X100 (non-ionic).

4.5 Permeability

As discussed in Section 2.1.2, Darcy's law can be employed to obtain the permeability of the membrane for the different surfactant solutions. The volumetric flow can be converted to flux by dividing both sides of the equation by the effective cross-sectional membrane area, yielding Equation 7.

$$J = \frac{k}{\mu}\frac{\delta p}{\delta x} \tag{7}$$

The equation above can be rewritten to an expression for the permeability κ:

$$\kappa = \frac{Q}{A\delta p}\,\mu\delta x \tag{8}$$

The dynamic viscosity for the surfactant solutions are not known, so an estimation will be made by assuming the viscosity of water for each solution: 0.890 mPa s at 25°C [27]. The thickness of membrane I (δx) is equal to 130 μm (Section 4.1). By linearly fitting the LLDP results of the first run (or combined first runs) for prewet membranes, the slope can determined and the permeability can be calculated for each surfactant. The results are shown in Table 7.

Table 7: Permeabilities of the prewet PVDF membrane to different solutions.

Solution	Slope [$\frac{m^3/m^2 s}{bar}$]	Permeability [darcy]
Water	0.030	0.035
SDS	0.037	0.043
CTAB	0.038	0.045
Triton	0.040	0.047

It should be noted however, that the prewet results were not completely linear (Appendix 7.2). The deviation from linearity at higher pressures suggests membrane compaction as the cause for this. Furthermore, in reality the viscosity will in all likelihood be affected by the presence of surfactants and temperature variance, so the calculated permeabilities may differ slightly from reality.

4.6 Microfluidic chip

Below, the analysed LCSM results are shown. No reliable SDS measurement was obtained due to addional oil entering the system. As discussed in Section 3.6, the S_{nw} value is the fractual saturation value of the non-wetting phase, in this case: water. In Figure 32 S_{nw} is shown as a function of time and place in the microfluidic chip. For Figure 33, the average values of each slice are taken. The slices are taken vertically for each x-coordinate.

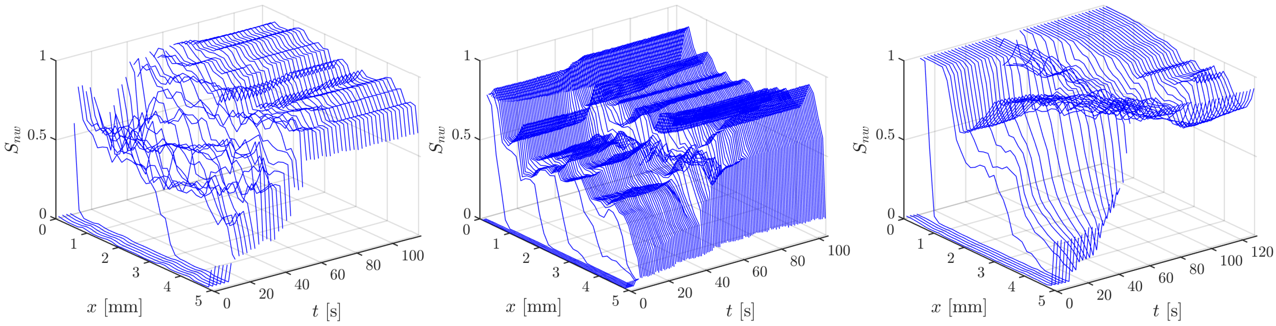

(a) CTAB solution (cationic).

(b) Triton X100 solution (non-ionic).

(c) DDAPS solution (zwitterionic).

Figure 32: Water saturation as a function of time and place (x) for different surfactant solutions through a SO AR20 infused microfluidic chip.

Amounts of remaining silicone oil in the microfluidic chip can be recognised as lower S_{nw} values in Figure 32. For DDAPS (Figure 32c) it can be seen than initially a large portion of the microfluidic chip is still infused with oil at the top of the chip, around x = 5 mm. At the same time, very high saturation values are observed at the other side of the chip: almost 100%. This preferential flow path temporarily prevents oil from being washed away in one section of the chip, but after some time most of the oil is also removed from that section.
It can be observed in Figure 32 and Figure 33 that a very large portion of the oil is removed within 2 minutes

for all surfactants. This effect is strongest for DDAPS, where most of the oil is removed. For CTAB, a larger amount of oil is retained and for Triton the largest amount of oil is left in the chip after the measurements. Nevertheless, a small but stable amount of residual oil is retained in every case.

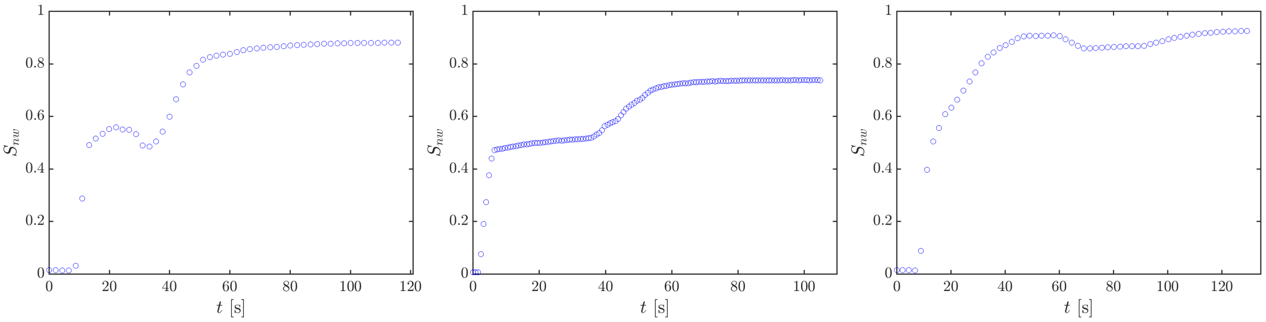

(a) CTAB solution.

(b) Triton X100 solution.

(c) DDAPS solution.

Figure 33: Water saturation as a function of time for different surfactant solutions through a SO AR20 infused microfluidic chip.

It can be seen in Figure 33 that the value of S_nw would sometimes decrease. The cause for this is additional droplets of silicone oil leaking into the inlet of the microfluidic chip and disturbing the measurements, as shown for DDAPS in Figure 34. Partly, the problem was caused by additional oil leaking into the systems, but sometimes also oil would remain at the side of the inlet and shoot loose in the middle of a measurement. For an accurate analysis, this should be prevented, for example by another chip design that decreases this effect.

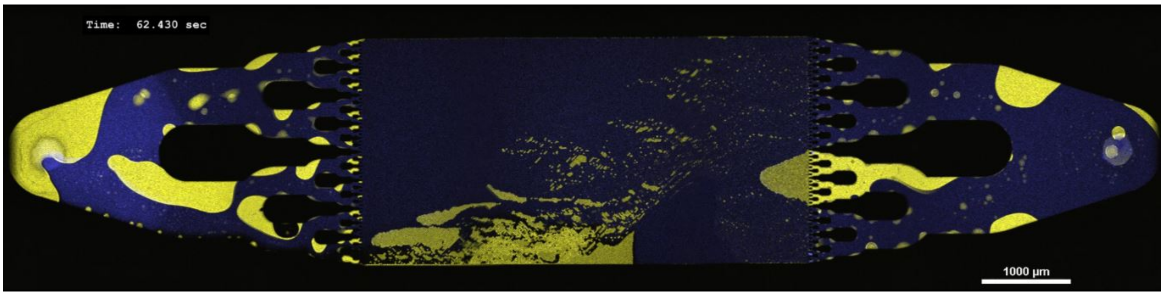

Figure 34: DDAPS solution pushing through silicone oil (AR20) in the microfluidic chip, while additional oil enters the chip (flow occurs from right to left).

4.7 Contact Angle Measurements

The advancing contact angle of pure water on the dense membrane was measured to be 122°.

Unfortunately, the dense membrane used for measuring the (advancing) contact angles was not completely dense. Because of the low surface tensions for the surfactant solutions, the dense membrane was infiltrated by the solutions yielding very unstable results. The observed effect of surfactant solution wicking into the dense membrane occurred faster for ARCA measurements than for the static contact angle measurements. Because of this, only the contact angle for pure water is known.

4.8 SFT prediction

In order to show the possibilities of LLDP measurements as a way of characterizing membranes, the SFT of water in air is predicted from the LLDP measurement. By presenting the data inversely (flux as a function of pressure), the parallels with GLDP can easily be seen, see Figure 35. Measurement points of the first runs are taken to construct the wet curve, while measurement points of the final 70% run are taken as the dry curve. As with GLDP, the intersection of the half-dry curve with the wet curve yields the pressure at which the Mean Flow Pore (MFP) sizes are opened. Because the MFP (1.26 μm, Section 4.2) and advancing contact angle on a dry membrane (142°) are known, the Laplace equation can be employed to calculate the surface tension: 75 mN/m, which is very close to the known value of 72 mN/m.
However, the advancing contact angle of water on a *dense* membrane should actually be used (122°) which results in $\gamma = 111$ mN/m, far from the real value.

It stands to reason that predicted values using this technique should not unthinkingly be accepted, as the contact angle has a very large effect on the final value.

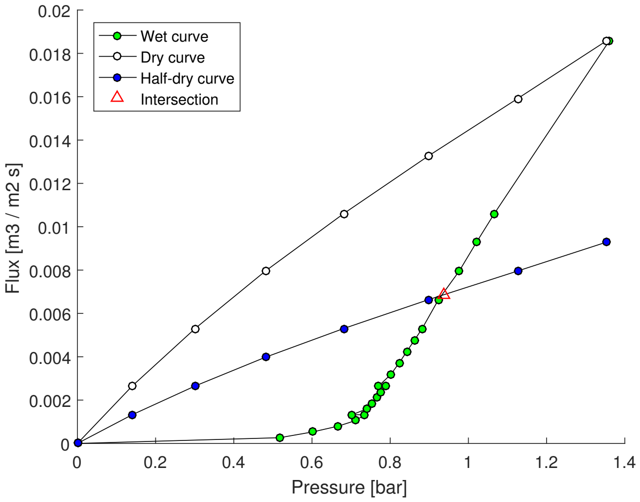

Figure 35: LLDP results for a dry membrane with MQ, which can be used for IFT prediction if the contact angle is known.

5 Conclusion

From the microfluidic experiments, it can be concluded that a large portion of silicone oil is swiftly washed away from the microfluidic chip by all tested surfactants, but still some oil remains and the final saturation value is rather stable. The results suggest DDAPS (zwitterionic) is the most harsh surfactant for silicone oil.

The LLDP results agree with the notion of remaining oil. It was observed that a certain amount of infusion liquid is retained up to the highest fluxes for all surfactant solutions. This assertion is mostly based on a qualitative comparison between pressures for dry and prewet membranes with SLIMs. For a more thorough understanding of SLIMs, however, this comparison would have to be quantified. For this, the advancing contact angle on dense membranes, and interfacial tensions of silicone oil with surfactant solutions, should be known, although these are difficult to measure due to physical limitations. Additionally, the possibility that other phenomena cause the higher SLIM pressures, should be ruled out with more research. This would make the conclusion, which is based mostly on the pressure difference between prewet and liquid infused membranes, more accurate. Examples of these phenomena include the formation of emulsions and the accumulation of undissolved surfactants causing repulsive interactions.

Finally, reasonable fitting with the Interfacial Pore Flow model is obtained for most of the experimental data. For some of the data, no fit was obtained, while the shape of the data did resemble the theoretical curve but at lower pressures. Therefore, it might still be possible to obtain a fit for these data with some modifications in the tolerance and fitting parameters.

6 Future work and recommendations

Firstly, it is difficult to make an accurate comparison of non-ionic surfactant versus different kinds of ionic ones. The surfactant concentrations as well as their (ratio to) CMC value differ. These differences cannot be quantitatively accounted for yet, due to missing information about contact angles and interfacial tensions. Also, the measurements are not always in complete agreement with the theory, presumably because of e.g. pores that are already opened at higher fluxes and the heterogeneous membrane structure. For this reason, it could be interesting to experimentally compare surfactants that are similar in ratio to CMC value but different in charge, to see in more detail the effect of surfactant charge on SLIM stability.

Secondly, for a more relevant application of the Interfacial Pore Flow model, it would be interesting to look at higher membrane pressures. However, this would require equipment capable of withstanding these higher pressures: a stronger liquid reservoir and tubing, as well as a suitable pressure meter. The saturation and bubble problems that nitrogen produce would worsen at higher pressures, so helium gas (while more expensive) would be the preferred pressurising medium.

Thirdly, it would be interesting to remeasure some of the high flux values with surfactant solution that is prepared using the new dispenser machine. If surfactants that are dissolved with this harsh machine (and at high temperatures) still yield the pressure buildup that was sometimes observed, it can be ruled out with more certainty that accumulation of undissolved surfactant particles cause pore clogging. Likewise, the influence of pressure instability could be investigated further, for example by varying the measurement time per step (currently 100 s) and see if pressure buildups are still observed.

References

[1] Xu Hou, Yuhang Hu, Alison Grinthal, Mughees Khan, and Joanna Aizenberg. Liquid-based gating mechanism with tunable multiphase selectivity and antifouling behaviour. *Nature*, 519(7541):70–73, Mar 2015. ISSN 0028-0836. URL `http://dx.doi.org/10.1038/nature14253`. Letter.

[2] Tak-Sing Wong, Sung Hoon Kang, Sindy K. Y. Tang, Elizabeth J. Smythe, Benjamin D. Hatton, Alison Grinthal, and Joanna Aizenberg. Bioinspired self-repairing slippery surfaces with pressure-stable omniphobicity. *Nature*, 477(7365):443–447, Sep 2011. ISSN 0028-0836. doi: 10.1038/nature10447. URL `http://dx.doi.org/10.1038/nature10447`.

[3] Moyuan Cao, Dawei Guo, Cunming Yu, Kan Li, Mingjie Liu, and Lei Jiang. Water-repellent properties of superhydrophobic and lubricant-infused "slippery" surfaces: A brief study on the functions and applications. *ACS Applied Materials & Interfaces*, 8(6):3615–3623, 2016. doi: 10.1021/acsami.5b07881. URL `http://dx.doi.org/10.1021/acsami.5b07881`. PMID: 26447551.

[4] Geoffrey Barnes and Ian Gentle. *Interfacial science: an introduction*. Oxford University Press, Oxford, 2011.

[5] Wikipedia. Wetting, 2017. URL `https://en.wikipedia.org/w/index.php?title=Wetting&oldid=774059767`. [Online; accessed 18-April-2017].

[6] Nurxat Nuraje, Waseem S. Khan, Yu Lei, Muhammet Ceylan, and Ramazan Asmatulu. Superhydrophobic electrospun nanofibers. *J. Mater. Chem. A*, 1:1929–1946, 2013. doi: 10.1039/C2TA00189F. URL `http://dx.doi.org/10.1039/C2TA00189F`.

[7] Surjyasish Mitra, Naga Siva Kumar Gunda, and Sushanta K. Mitra. Wetting characteristics of underwater micro-patterned surfaces. *RSC Adv.*, 7:9064–9072, 2017. doi: 10.1039/C6RA25888C. URL `http://dx.doi.org/10.1039/C6RA25888C`.

[8] Hanieh Bazyar, Sirus Javadpour, and Rob G. H. Lammertink. On the gating mechanism of slippery liquid infused porous membranes. *Advanced Materials Interfaces*, 3(14):1600025–n/a, 2016. ISSN 2196-7350. doi: 10.1002/admi.201600025. URL `http://dx.doi.org/10.1002/admi.201600025`. 1600025.

[9] Wikipedia. Contact angle, 2017. URL `https://en.wikipedia.org/w/index.php?title=Contact_angle&oldid=783553447`. [Online; accessed 07-June-2017].

[10] Hanieh Bazyar. Investigation of immiscible liquid-liquid displacement in slippery liquid infused membranes (slim) – a microfluidic study (research description), 2017.

[11] Enrique Antón, José Ignacio Calvo, José R. Álvarez, Antonio Hernández, and Susana Luque. Fitting approach to liquid–liquid displacement porosimetry based on the log-normal pore size distribution. *Journal of Membrane Science*, 470:219 – 228, 2014. ISSN 0376-7388. doi: http://dx.doi.org/10.1016/j.memsci.2014.07.035. URL `http://www.sciencedirect.com/science/article/pii/S037673881400564X`.

[12] Sigma. Product information: Triton x-100, 2017. URL `https://www.sigmaaldrich.com/content/dam/sigma-aldrich/docs/Sigma/Product_Information_Sheet/1/x100rspis.pdf`. [Online; accessed 25-June-2017].

[13] Tulasi Niraula, Ajaya Bhattarai, and Sujeet Chatterjee. Critical micelle concentration of sodium dodecyl sulphate in pure water and in methanol-water mixed solvent media in presence and absence of kcl by surface tension and viscosity methods. *BIBECHANA*, 11(0):103–112, 2014. ISSN 2382-5340. URL `http://dx.doi.org/10.3126/bibechana.v11i0.10388`.

[14] Sigma. Product information: Hexadecyltrimethylammonium bromide, 2017. URL `https://www.sigmaaldrich.com/content/dam/sigma-aldrich/docs/Sigma/Product_Information_Sheet/2/h6269pis.pdf`. [Online; accessed 25-June-2017].

[15] Sigma. N-dodecyl-n,n-dimethyl-3-ammonio-1-propanesulfonate, 2017. URL `http://www.sigmaaldrich.com/catalog/product/sigma/d0431?lang=en&region=NL`. [Online; accessed 25-June-2017].

[16] DuPont. Krytox performance lubricants - product information, 2017. URL `http://www2.dupont.com/Lubricants/en_US/assets/downloads/H-58510-5_Krytox_Typical_Properties.pdf`. [Online; accessed 25-June-2017].

[17] Sigma. Silicone oil ar 20, 2017. URL `http://www.sigmaaldrich.com/catalog/product/aldrich/10836?lang=en&region=NL`. [Online; accessed 25-June-2017].

[18] Ray F. Egerton. *An Introduction to Microscopy*, pages 1–25. Springer US, Boston, MA, 2005. ISBN 978-0-387-26016-7. doi: 10.1007/0-387-26016-1_1. URL http://dx.doi.org/10.1007/0-387-26016-1_1.

[19] Porometer. Porolux 1000 series, 2017. URL http://www.porometer.com/porometers/instruments/porolux-1000/. [Online; accessed 21-June-2017].

[20] Yong Tang, Ruizhi Yang, Zhimin Du, and Fanhua Zeng. Experimental study of formation damage caused by complete water vaporization and salt precipitation in sandstone reservoirs. *Transport in Porous Media*, 107(1):205–218, 2015. ISSN 1573-1634. doi: 10.1007/s11242-014-0433-1. URL http://dx.doi.org/10.1007/s11242-014-0433-1.

[21] European Membrane Institute (EMI) Twente. Capillary flow porometry, 2017. URL https://www.utwente.nl/en/tnw/emi/facilities/characterisation/porometry/. [Online; accessed 06-June-2017].

[22] José Ignacio Calvo, René Israel Peinador, Pedro Prádanos, Laura Palacio, Aldo Bottino, Gustavo Capannelli, and Antonio Hernández. Liquid–liquid displacement porometry to estimate the molecular weight cut-off of ultrafiltration membranes. *Desalination*, 268(1):174 – 181, 2011. ISSN 0011-9164. doi: http://dx.doi.org/10.1016/j.desal.2010.10.016. URL http://www.sciencedirect.com/science/article/pii/S0011916410007319.

[23] Shinya Inoué. *Foundations of Confocal Scanned Imaging in Light Microscopy*, pages 1–19. Springer US, Boston, MA, 2006. ISBN 978-0-387-45524-2. doi: 10.1007/978-0-387-45524-2_1. URL http://dx.doi.org/10.1007/978-0-387-45524-2_1.

[24] Dataphysics. Pendant drop method, 2017. URL http://www.dataphysics.de/2/start/understanding-interfaces/drop-shape-analysis/pendant-drop-method/. [Online; accessed 25-June-2017].

[25] Wikipedia. Wilhelmy plate, 2017. URL https://en.wikipedia.org/w/index.php?title=Wilhelmy_plate&oldid=775240161. [Online; accessed 25-June-2017].

[26] Motoyasu Kobayashi, Yuki Terayama, Hiroki Yamaguchi, Masami Terada, Daiki Murakami, Kazuhiko Ishihara, and Atsushi Takahara. Wettability and antifouling behavior on the surfaces of superhydrophilic polymer brushes. *Langmuir*, 28(18):7212–7222, 2012. doi: 10.1021/la301033h. URL http://dx.doi.org/10.1021/la301033h. PMID: 22500465.

[27] John C. Crittenden, R. Rhodes Trussell, David W. Hand, Kerry J. Howe, and George Tchobanoglous. *Appendix C: Physical Properties of Water*, pages 1861–1862. John Wiley & Sons, Inc., 2012. ISBN 9781118131473. doi: 10.1002/9781118131473.app3. URL http://dx.doi.org/10.1002/9781118131473.app3.

7 Appendices

On the next pages, the appendices can be found.

7.1 Appendix A: LLDP results

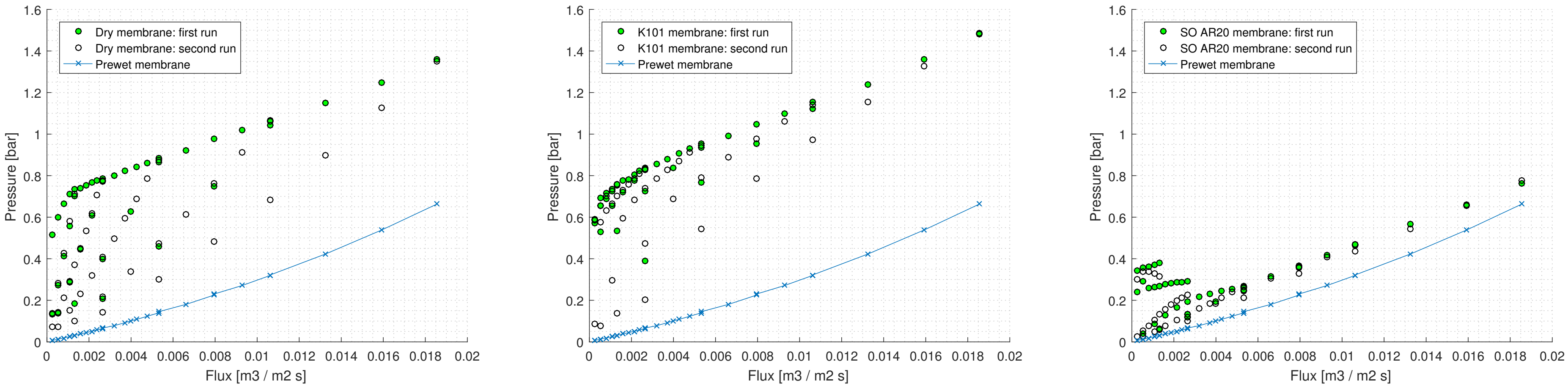

(a) Dry membrane with MQ.

(b) Krytox 101 infused membrane with MQ.

(c) Silicone oil AR20 infused membrane with MQ.

Figure 36: The analysed LLDP results for pure water (MQ).

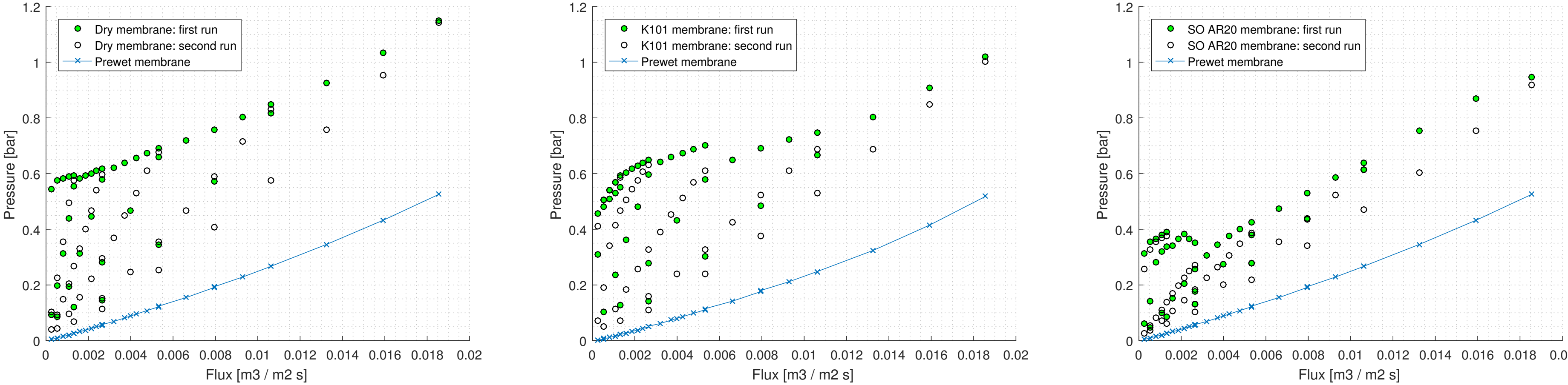

(a) Dry membrane with SDS solution.

(b) Krytox 101 infused membrane with SDS solution.

(c) Silicone oil AR20 infused membrane with SDS solution.

Figure 37: The analysed LLDP results for SDS (anionic).

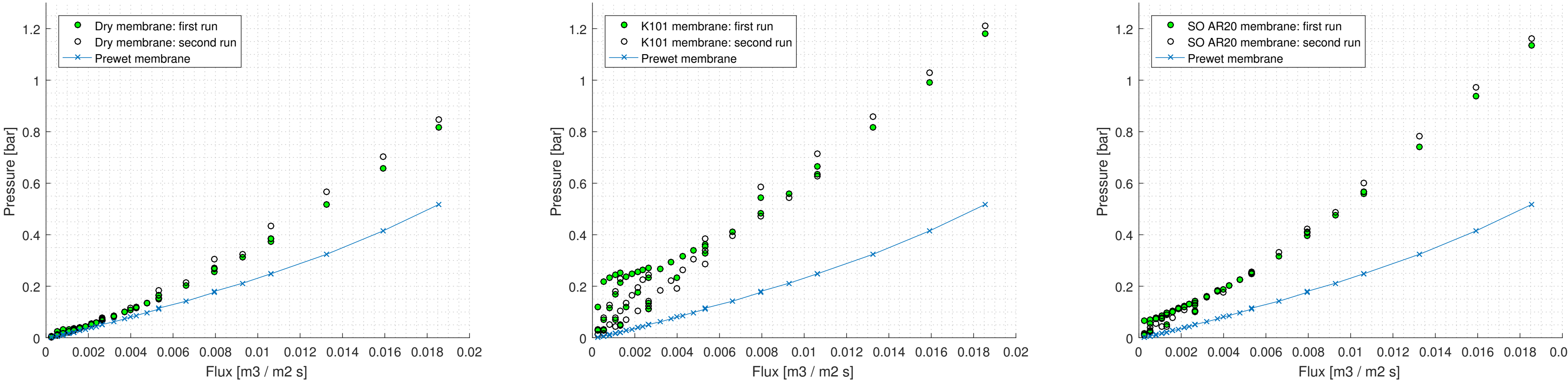

(a) Dry membrane with CTAB solution.

(b) Krytox 101 infused membrane with CTAB solution.

(c) Silicone oil AR20 infused membrane with CTAB solution.

Figure 38: The analysed LLDP results for CTAB (cationic).

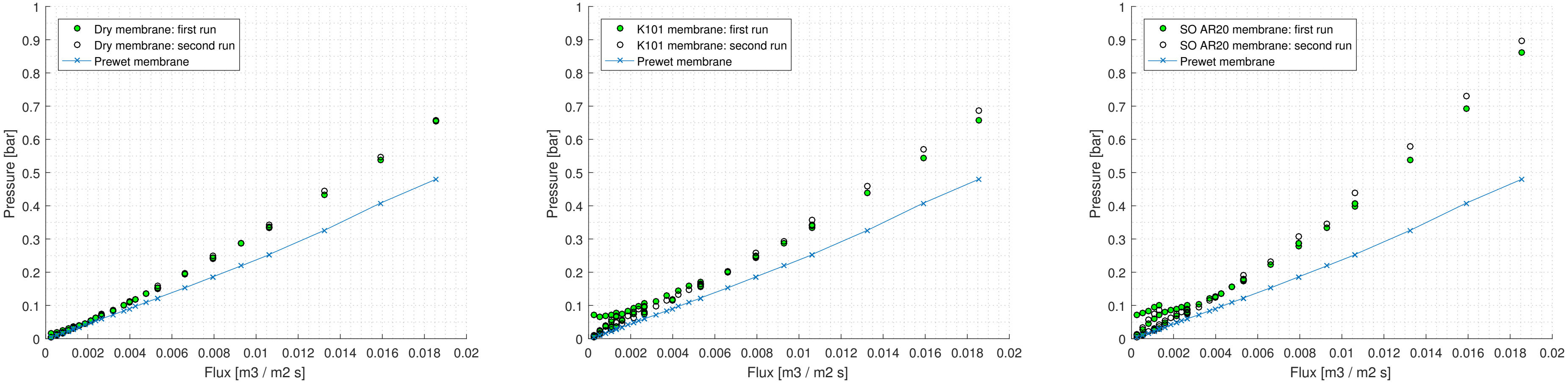

(a) Dry membrane with Triton X100 solution.

(b) Krytox 101 infused membrane with Triton X100.

(c) Silicone oil AR20 infused membrane with Triton X100.

Figure 39: The analysed LLDP results for Triton X100 (non-ionic).

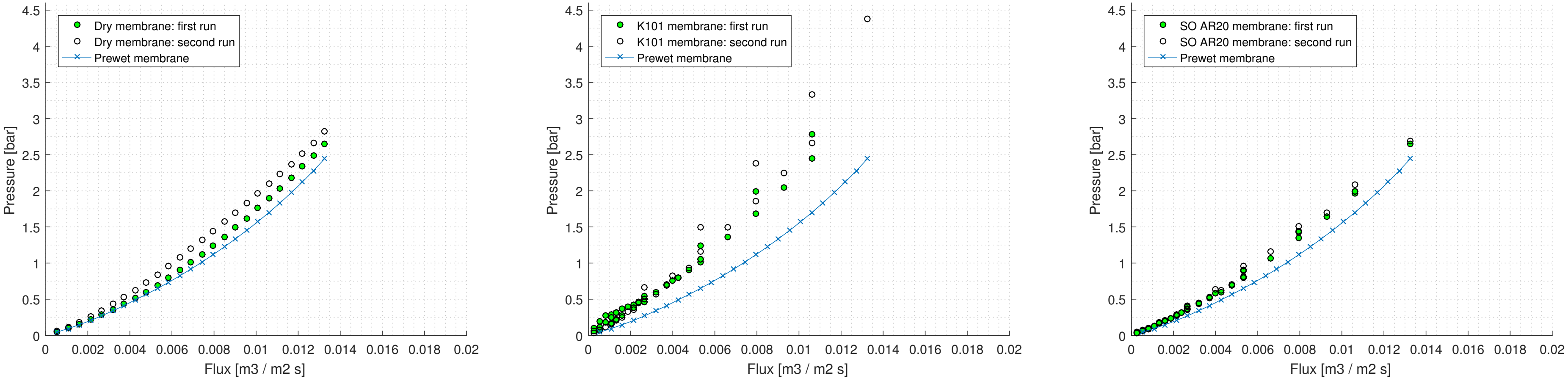

(a) Dry membrane with DDAPS solution.

(b) Krytox 101 infused membrane with DDAPS solution.

(c) Silicone oil AR20 infused membrane with DDAPS.

Figure 40: The analysed LLDP results for DDAPS (zwitterionic).

7.2 Appendix B: Prewet LLDP results

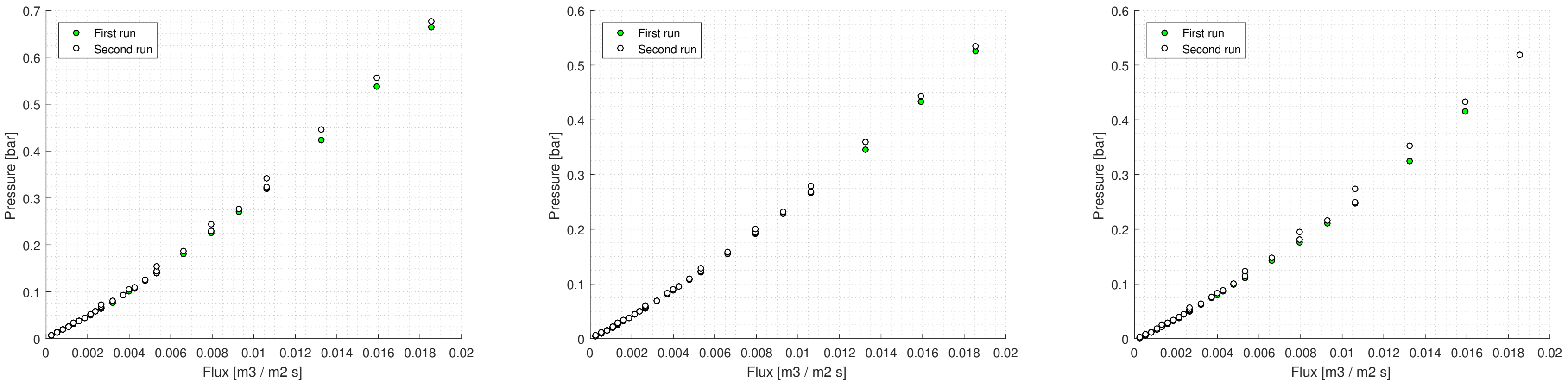

(a) Prewet membrane measured with MQ.

(b) Prewet membrane measured with SDS solution.

(c) Prewet membrane measured with CTAB solution.

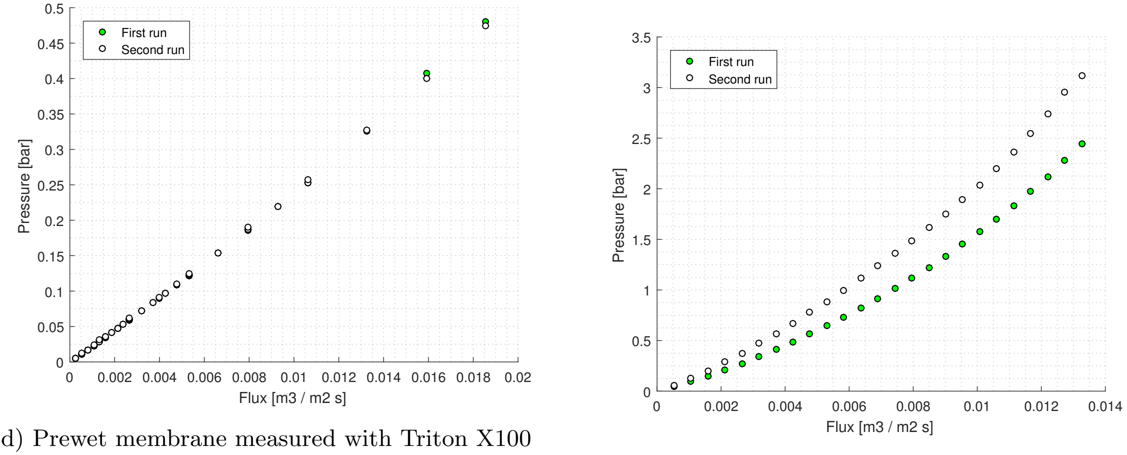

(d) Prewet membrane measured with Triton X100 solution.

(e) Prewet membrane measured with DDAPS solution.

Figure 41: LLDP results for prewet membranes.